International Journal of Nanomedicine

Dovepress
Taylor & Francis Group

Open Access Full Text Article

ORIGINAL RESEARCH

Chondroitin Sulphate-Chitosan Based Nanogels Loaded with Naringenin-β-Cyclodextrin Complex as Potential Tool for the Treatment of Diabetic Retinopathy: A Formulation Study

Gaia Zucca[1], Barbara Vigani[1], Caterina Valentino[1], Marco Ruggeri[1], Nicoletta Marchesi[1], Alessia Pascale[1], Giulia Giovilli[2], Lorenzo Malavasi[2], Giuseppina Sandri[1], Silvia Rossi[1]

[1]Department of Drug Sciences, University of Pavia, Pavia, 27100, Italy; [2]Department of Chemistry and INSTM, University of Pavia, Pavia, 27100, Italy

Correspondence: Silvia Rossi; Barbara Vigani, Department of Drug Sciences, University of Pavia, Via Taramelli 12, Pavia, 27100, Italy, Email silvia.rossi@unipv.it; barbara.vigani@unipv.it

Purpose: The main purpose of the study was the formulation development of nanogels (NHs) composed of chondroitin sulfate (CS) and low molecular weight chitosan (lCH), loaded with a naringenin-β-cyclodextrin complex (NAR/β-CD), as a potential treatment for early-stage diabetic retinopathy.

Methods: Different formulations of NHs were prepared by varying polymer concentration, lCH ratio, and pH and, then, characterized for particle size, zeta potential, particle concentration (particles/mL) and morphology. Cytotoxicity and internalization were assessed in vitro using Human Umbilical Vein Endothelial Cells (HUVEC). The NAR/β-CD complex was prepared and evaluated for morphology, complexation efficiency, and solubility. Finally, the most promising NH prototype was loaded with NAR/β-CD (NH@NAR/β-CD) and further characterized for encapsulation efficiency, loading capacity, opacity and cytotoxicity on HUVEC; in vitro release test and DPPH assay were performed to investigate NH capability to sustain NAR release and NH@NAR/β-CD antioxidant properties, respectively.

Results: NH properties were influenced by polymer concentration, lCH ratio, and pH. N3 (0.5 mg/mL; lCH=1.5:1; pH = 5) and N9 (0.5 mg/mL; lCH=1:1; pH = 5) showed optimal characteristics, including small size (<350 nm) and positive zeta potential, facilitating cellular uptake. The NAR/β-CD complex showed 71% complexation efficiency and enhanced NAR solubility. Since characterized by superior properties and better in vitro biocompatibility, N3 was loaded with NAR/β-CD. N3@NAR/β-CD capability to sustain in vitro NAR release, radical scavenging activity and in vitro biocompatibility were finally demonstrated.

Conclusion: The physico-chemical properties of N3@NAR/β-CD were responsible for their cell uptake, suggesting their potential to target retinal endothelial cells. The high NAR/β-CD complexation efficiency and the sustained NAR release over 72 hours could guarantee the maintenance of an effective drug concentration at the damage site while reducing the injection number. Further studies about the safety and the effectiveness of the intravitreal injection of NHs@NAR/β-CD will be performed on a diabetic animal model.

Keywords: polyelectrolyte complexation, cellular uptake, inclusion complex, antioxidant properties, intravitreal administration

Introduction

Diabetes mellitus is a chronic disease which approximately affects 422 million people worldwide.[1] The most widespread complication of this pathology is the diabetic retinopathy (DR), a disease affecting the posterior segment of the eye known to be globally the main cause of vision impairment or loss among adults of working age and elderly people.[2–4] The pathophysiology of DR involves a progressive damage of retinal blood vessels due to a persistent hyperglycemic state.[5–7] Particularly, it has been reported that hyperglycemia-induced oxidative damages in the retina are related to modifications of several metabolic pathways and result in two main different molecular mechanisms: i) an increase in the synthesis of the Vascular Endothelial Growth Factor (VEGF), promoting the process of neoangiogenesis and, thus, the

Received: 24 July 2024
Accepted: 21 December 2024
Published: 22 January 2025

Graphical Abstract

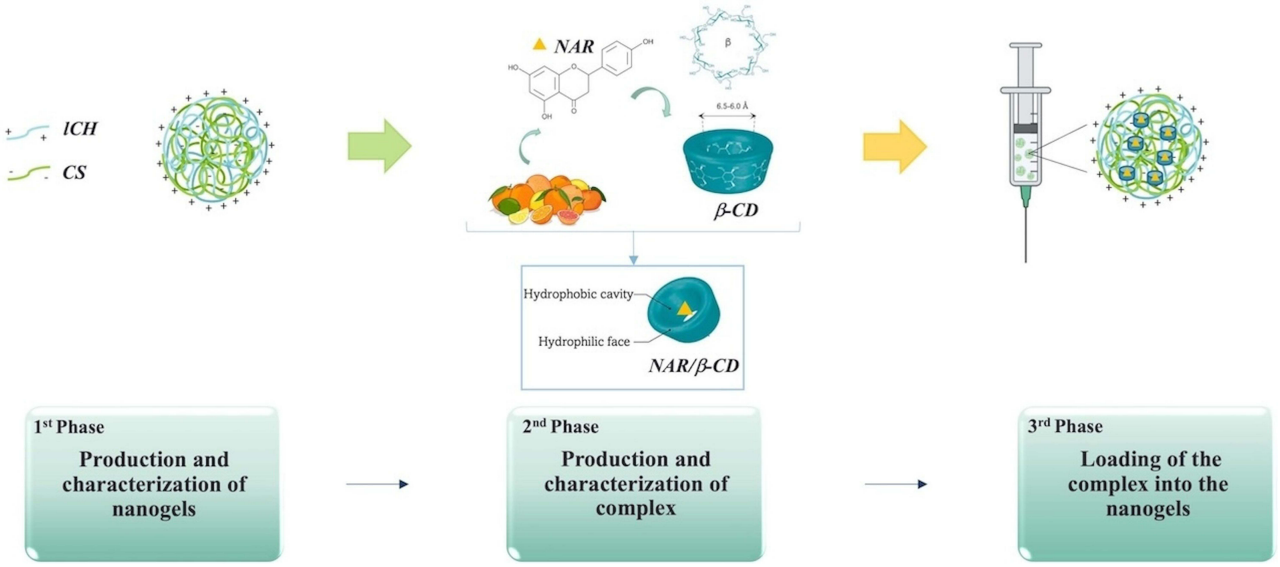

development of new blood vessels in the retina and ii) an increase in the intracellular levels of reactive oxygen species (ROS).[4,8,9]

Naringenin (NAR) is a polyphenolic compound, abundantly found in citrus fruits, that is well known for its pharmacological activities, such as antidiabetic, anti-cancer, anti-inflammatory and antioxidant properties.[10–12] Moreover, different authors have reported that NAR exhibited beneficial effects in the management of ocular disorders, such as diabetes-induced retinal damage.[13] According to several studies on streptozotocin-induced diabetic rat model, NAR may reduce the retinal damage caused by oxidative stress through i) the activation of the Nrf2/ARE signaling pathway that plays a key role in maintaining intracellular redox homeostasis, regulating inflammatory damage, and alleviating retinal cytotoxicity;[13,14] ii) the reduction of lipid peroxidation, which is responsible for retinal cell apoptosis;[15,16] iii) the restoration of normal glutathione levels, a crucial endogenous antioxidant.[17,18] Nevertheless, the above-mentioned biological properties are hindered by NAR hydrophobic nature, which is responsible for its poor water solubility.[12,19] The preparation of inclusion complexes between NAR and cyclodextrins (CDs), which are torus-shaped oligosaccharides composed of α-(1,4)-linked glucose units, has been proposed in the literature as a strategy to enhance NAR solubility in aqueous media.[20–22] In general, β-CD is the most widely used type of CDs for improving the solubility, the stability, and the bioavailability of poorly water-soluble molecules.[23–26]

Delivering drugs to retina remains a significant challenge due to the anatomical and physiological barriers of the ocular structure.[27,28] Current treatments of DR include intravitreal injections of solutions containing conventional drugs (ie corticosteroids, nonsteroidal anti-inflammatory drugs, antioxidants, and anti-VEGF) and retinal surgeries (ie laser treatment and vitrectomy). These approaches primarily manage the symptoms of the advanced stages of DR, but fail to prevent its onset and progression.[29] Moreover, in order to maintain drug therapeutic concentrations in the posterior segment over time, conventional therapies require repeated intravitreal injections, which are poorly tolerated by patients and may carry inherent risks, including endophthalmitis, cataract formation, retinal detachment, and vitreous hemorrhage.[24,29,30] The limitations of the intraocular modalities and the risks associated with major surgeries (ie vitreous hemorrhage, cataract, and neovascular glaucoma) have driven interest in the use of innovative drug delivery systems.[31,32]

In this context, the intravitreal administration of nanosystems (NSs) could represent a promising approach to overcome the drawbacks of the current treatments. Specifically, NSs have been shown to prolong the release and to enhance targeted delivery of the loaded drugs, reducing the number of injections and, thus, modulating side effects. In

addition, NSs represent versatile drug delivery systems due to their tunable physico-chemical properties and the ease of surface modification that allow site-specific delivery.[31–36] Recently, polymer-based nanoparticles have been proposed as drug delivery systems for managing DR upon intravitreal administration: nanoparticles based on synthetic polymers (ie poly (lactic-co-glycolic acid), polycaprolactone) and natural ones (ie chitosan, hyaluronic acid) have been reported for the delivery of monoclonal antibodies (ie bevacizumab), corticosteroids (ie triamcinolone acetonide) and antioxidant plant-derived molecules (ie resveratrol, lutein).[37–41]

Nanogels (NHs) are a type of polymer-based nanoparticles, composed of a three-dimensional network of polyelectrolyte chains formed through physical entanglements and electrostatic interactions between opposite charges; among polymer-based nanoparticles, NHs have gained interest due to the ease of preparation, the ability to encapsulate both hydrophilic and hydrophobic drugs, and their large surface area and porous structure, which enable high encapsulation efficiency.[42–44]

Chitosan (CH) is a natural mucopolysaccharide derived from the alkaline deacetylation of chitin, mainly obtained from the exoskeleton of marine invertebrates.[45,46] Both the physico-chemical properties and the bioactivity of CH are influenced by its degree of deacetylation and molecular weight (MW). As a consequence of the deacetylation process, CH exhibits a cationic nature and water solubility at acidic pH values, due to the protonation of its free amino groups. This feature is responsible for many different properties, such as the formation of ionic interactions with a vast number of negatively charged molecules and the capacity for enhancing permeation.[47–49] Moreover, it has been reported that CH is characterized by antioxidant activity, strongly related to its MW: shorter CH chains have a lower tendency of forming intramolecular hydroxyl bonds, leading to a higher availability of activated hydroxyl and amino groups that support the radical scavenging action.[50,51]

Chondroitin sulphate (CS) is a naturally occurring macromolecule classified as glycosaminoglycans (GAGs), characterized by a net negative charge.[52,53] It is extensively present in animal tissues extracellular matrix, holding a pivotal role in preserving organ and tissue integrity. Due to its anti-inflammatory, antioxidant, and anti-apoptotic effects, it finds widespread use for bone enhancement and dry eye treatment.[54,55]

Given these premises, the present work is focused on the formulation development of NHs, composed of CS and low MW CH (lCH) and loaded with an inclusion complex between β-CD and NAR (NAR/β-CD). Such NHs could be administered by intravitreal injection as potential tool for the treatment of the retinal damage caused by oxidative stress during the early stages of DR. In this context, to the best of our knowledge, it is the first time that NHs, composed of polymers with well known antioxidant properties, have been proposed as NAR/β-CD delivery systems.

The NHs formation occurs throughout the polyelectrolytic complexation method between the cationic and anionic sites of lCH and CS polymeric chains, respectively. Different experimental variables (ie the total polymer concentration, the lCH:CS ratio and the pH values) were considered to obtain NHs in a size range useful to allow the diffusion through the vitreous and the endothelial cellular uptake.[35,36,56] NHs thus obtained were characterized in terms of particle size, zeta potential, concentration and morphology; preliminary short-term stability studies were also performed. Finally, NHs were evaluated in vitro for their biocompatibility and capability to be internalized by the cells using Human Umbilical Vein Endothelial Cells (HUVEC). For the NAR/β-CD complex preparation, different process conditions in terms of stirring time and reaction temperature were investigated. The NAR/β-CD complex was characterized for its morphological properties, complexation efficiency and NAR water solubility. Finally, the best NH prototype was loaded with the NAR/β-CD complex; NAR/β-CD-loaded NHs were evaluated in terms of particle size, zeta potential, loading capacity, encapsulation efficiency and opacity. In vitro release test was carried out to investigate the capability of NHs to sustain NAR release over time and the antioxidant activity of NAR/β-CD-loaded NHs was also evaluated using a DPPH assay. Finally, in vitro analyses on HUVEC cell line were performed to assess the biocompatibility of the final NHs dispersions.

Materials and Methods

Materials

For NHs preparation, chitosan (lCH, deacetylation grade 75%–85%, low molecular weight 50 kDa-190 kDa) and sodium hydroxide were purchased from Sigma-Aldrich (Milan, Italy); bovine chondroitin sulphate sodium salt 100 EP (CS, low molecular weight 14 kDa) was obtained from Bioiberica (Barcelona, Spain); glacial acetic acid was obtained from Carlo Erba (Milan, Italy).

For inclusion complex preparation, β-cyclodextrins (β-CD, 1135 g/mol) were provided by Giusto Faravelli S.p.A. (Milan, Italy); naringenin (NAR, 272.275 g/mol) was purchased by Sigma-Aldrich (Milan, Italy); ethanol absolute anhydrous was obtained from Carlo Erba (Milan, Italy).

Sigma Aldrich (Milan, Italy) was the supplier of all the materials used for in vitro studies on Human Umbilical Vein Endothelial Cells (HUVEC): all-in-one ready-to-use medium (Endothelial cell growth medium, CM), trypsin-EDTA solution, triazolyl blue tetrazolium bromide (MTT), dimethyl sulphoxide (DMSO), paraformaldehyde, tetramethylrhodamine B isothiocyanate (TRITC), TRITON-X 100 (TX100), bisbenzimide 3342 trichloride (HOECHST 3342), phosphate buffered saline (PBS) and trypan blue.

Preparation of lCH/CS Nanogels

NHs prototypes were prepared through the polyelectrolytic complexation method.[57] Briefly, two stocks solutions of low molecular weight chitosan (lCH) and chondroitin sulfate (CS) were prepared in 0.1 M acetic acid under magnetic stirring for 1 hour, at room temperature. Each solution was titrated to the desired pH value by progressive addition of 1 M NaOH, using a pHmeter (Mettler Toledo, SevenCompact, Columbus, Ohio, USA). Thereafter, CS solution was continuously extruded from a syringe with 25G needle into lCH one, maintained under vigorous and constant magnetic stirring for 10 minutes at room temperature. As reported in Table 1, different formulations (from N1 to N15) were prepared and three experimental variables were considered: i) the total polymer concentration (calculated as the sum of lCH and CS concentrations in the NHs dispersion), ii) the lCH:CS ratio (1.5:1, 3:1, 1:1 v/v) and iii) the pH value of the NHs dispersion (5.5, 4.0, 3.0).[57–62] Different pH values were selected to investigate how pH-dependent alternations of the degree of ionization and the charge density and distribution of the considered polymers (lCH and CS) could affect NHs physico-chemical properties: in fact, it is well known that pH can modulate both the protonation of lCH and the deprotonation of CS, thereby influencing their electrostatic interactions.

Table 1 Quali-Quantitative Composition (Expressed as mg/mL), lCH:CS Ratio (v/v) and pH Value of NHs

Formulation	Stock Solution Concentrations		Total Polymer Concentration	lCH:CS ratio (v/v)	pH
	lCH	CS			
N1	1	1	1	1.5:1	5.5
N2	0.75	0.75	0.75	1.5:1	5.5
N3	0.5	0.5	0.5	1.5:1	5.5
N4	1	1	1	3:1	5.5
N5	0.75	0.75	0.75	3:1	5.5
N6	0.5	0.5	0.5	3:1	5.5
N7	1	1	1	1:1	5.5
N8	0.75	0.75	0.75	1:1	5.5
N9	0.5	0.5	0.5	1:1	5.5
N10	1	1	1	1.5:1	3
N11	0.75	0.75	0.75	1.5:1	3
N12	0.5	0.5	0.5	1.5:1	3
N13	1	1	1	1.5:1	4
N14	0.75	0.75	0.75	1.5:1	4
N15	0.5	0.5	0.5	1.5:1	4

Characterization of lCH/CS Nanogels

Particle Size and Zeta Potential

NHs particle size and polydispersity index (PDI) were determined by dynamic light scattering (DLS) (Litesizer 500, Anton Paar, Turin, Italy). PDI indicates the width of the size distribution ranging between 0 (monodisperse system) and 1. The analysis were realized at 20°C with automatic measurement angle. For each formulation, three samples were analysed and, for each sample, three measurements were performed.

NHs zeta potential was investigated by electrophoretic light scattering (ELS) (Litesizer 500, Anton Paar, Turin, Italy); the analysis was conducted at 20°C with 2 minutes of equilibration time, Smoluchowski approximation, 1.50 of Henry factor, at 200 Volt. For each formulation, three samples were analysed and, for each sample, three measurements were performed.

Preliminary Short-Term Stability Studies

The physico-chemical stability of NHs prototypes, in form of colloidal dispersion, was evaluated by DLS and ELS analyses (Litesizer 500, Anton Paar, Turin, Italy) after storage at 4°C for 7 days. This stability study aimed to provide evidence that NHs physico-chemical properties did not significantly varied within 7 days of storage at 4°C and, thus, NHs could be used within that time for in vitro studies on cell models.

Nanoparticle Tracking Analysis

NHs prototype concentrations (particles/mL) were determined by nanoparticle tracking analysis using NanoSight Pro (NSPRO, Malvern Panalytical Ltd., Malvern, United Kingdom), fitted with a NSPRO flow-cell top plate and a 488 nm laser. The NanoSight sample pump was used in continuous flow with 1 mL syringes. NHs prototypes were diluted 1:1000 and 1:10,000 v/v in acetate buffer (namely 0.1 M acetic acid aqueous solution, then buffered with NaOH to a pH of 5.5) immediately prior to analysis. All measurements were carried out at 25°C with a detection angle of 90° in triplicate. A single analysis represented a fresh dilution of the stock NHs dispersion and consisted of three 29 ms video captures. Results were analysed with the NS XPLORER software (Malvern Panalytical, Malvern, United Kingdom).

Morphological Analysis

NHs prototypes morphology was investigated by means of a scanning electron microscope (SEM; Phenom™ Pure Desktop, Thermo Scientific, Waltham, Massachusetts, USA) and a transmission electron microscope (TEM; JEOL JEM-1200 EX II microscope; CCD camera Olympus Mega View G2, with 1376 × 1032-pixel format, Tokyo, Japan).

For SEM analysis, NHs prototype dispersion was centrifuged with Hermle Z326K (Wehingen, Germany) at 8000 rpm for 90 minutes at 20°C. Afterwards, the supernatant was removed and the remaining pellet, consisting of NHs prototypes, were subjected to freezing at −20°C for 24 hours and subsequent sublimation for 48 hours (Heto Dryer, Analytica De Mori, Milan, Italy). The freeze-dried NHs prototypes were thus placed on a steel stub and made conductive by the deposition of 10 nm of graphite under vacuum (sputtering). Images were obtained at low voltage, in high vacuum, at room temperature and at different magnifications (35 kX and 15 kX).

For TEM analysis, 10 µL of each NHs dispersion diluted 1:100 v/v in acetate buffer (pH = 5.5) were placed on TEM grids (formvar/carbon 300-mesh Cu, Agar Scientific, Monterotondo, Italy). Before the analysis, 10 µL of 2% v/v phosphotungstic acid aqueous solution (Sigma-Aldrich, Milan, Italy) were applied on the sample for 1 minute to provide contrast for better visualization of NHs prototype.[63] The analysis was performed with an acceleration voltage of 100 kV at room temperature; images were obtained at two different magnifications (40 kX and 100 kX).

FITC-Dex Encapsulation Efficiency Calculation

NHs prototypes were loaded with fluorescein isothiocyanate-dextran (FITC-dex, Sigma-Aldrich, Milan, Italy) as a fluorescent probe. Briefly, FITC-dex was added to lCH solution to reach a concentration equal to 1 mg/mL. FITC-dex-loaded NHs (NH@FITC-dex) were prepared as previously described in section "Preparation of lCH/CS nanogels".

A known volume of NH@FITC-dex NHs dispersion was centrifuged (8000 rpm for 90 minutes at 20°C); the fluorescence of the supernatant containing non-encapsulated FITC-dex (free FITC-dex) was measured by means of multi-mode microplate reader (FLUOstar Omega Microplate Reader, BMG LabTech, Ortenberg, Germany) at λ_{ex}= 490 nm and

λ_{em}= 520 nm. Supernatant FITC-dex concentration was determined by using a calibration curve obtained by preparing standard FITC-dex solutions at known and increasing concentrations (0.1–1 mg/mL) in acetate buffer (pH = 5.5). Once quantified the amount of free FITC-dex into the supernatant (W_{free}), the encapsulation efficiency (EE%) was calculated by the following equation:

$$EE\,\% = \frac{W_{en}}{W_0} * 100$$

where W_0 was the initial amount of FITC-dex added to the NHs dispersion and W_{en} was the amount of FITC-dex loaded into the NHs (W_0-W_{free}). All experiments were carried out in triplicate.

Cytotoxicity Test

The cytotoxicity of NHs prototypes was assessed on HUVEC cells, which are widely used in the literature to demonstrate stimulation-dependent angiogenesis and key endothelial cell signaling pathways involved in diabetic retinopathy.[64–66] Cells (p7-p10) were cultured in polystyrene flasks in CM and incubated at 37°C in 5% CO_2 atmosphere and 95% of relative humidity (RH). Next, 100 µL of cell suspension was seeded in 96-wells plate (25,000 cells/mL); after 24 hours, 100 µL of NHs dispersions, diluted in CM at 1:10, 1:25, 1:50 and 1:100 v/v, were introduced in each well and left in contact with cells for 24 hours. Finally, a MTT assay was performed to evaluate NHs cytotoxicity. Briefly, after removal of samples and rinsing each well with PBS, 50 µL of MTT (1 mg/mL) in PBS and 100 µL of CM were added to each well and incubated for 3 hours (37°C, 5% CO_2, 95% RH). Subsequently, 100 µL of DMSO, used as solubilizing agent, was added to each well, in order to promote the complete dissolution of formazan crystals, obtained from MTT dye reduction effected by mitochondrial dehydrogenases of living cells. The solution absorbance was measured by means of a Synergy HT spectrophotometer (BioTek Instruments, Winooski, Vermont, USA) at 595 nm wavelength, after 10 min of shaking. Results were expressed as % cell viability by normalizing the absorbance measured after contact with each sample with that measured after contact with CM alone, used as reference. Six replicates were performed for each sample.

Cellular Uptake

Cells were plated (60,000 cells/well) on microscope glass coverslips (22x22 mm) and treated for 3 hours with NH@FITC-dex NHs diluted 1:25 v/v with CM or with CM alone as control. Subsequently, cells were washed with PBS and treated with 1 mL of 4% v/v paraformaldehyde solution for 20 minutes. After washing with PBS, cells were permeabilized with 0.1% v/v TX100 for 15 minutes at room temperature, rinsed with PBS and then, stained for actin fibers with 50 µL of TRITC solution (50 µg/mL) for 45 minutes at room temperature in the dark. After rinsing with PBS, cells were stained for DNA with Hoechst 33342 solution (0.1 µg/mL) for 10 min at room temperature in the dark. After rinsing with PBS, samples were observed using a Confocal Laser Scanning Microscope (CLSM, Leica TCS SP2, Leica Microsystems, Buccinasco, Italy) with λ_{ex}= 490 nm and λ_{em}= 520 nm for FITC-dex, λ_{ex}= 361 nm and λ_{em}= 497 nm for Hoechst 33342, and λ_{ex}= 514 nm and λ_{em}= 580 nm for TRITC. The acquired images were processed with a software associated with the microscope (Leica Microsystem, Buccinasco, Italy).

Preparation of NAR/β-CD Complexes

NAR/β-CD complexes were prepared according to the co-precipitation method starting from two stock solutions of naringenin (NAR) and β-CD, prepared in absolute ethanol (EtOH) and in MilliQ water, respectively (Figure 1). In detail, NAR solution (2.5 mm) was added to β-CD one (0.625 mm), under mild magnetic stirring (1:1 molar ratio) (1);[67,68] different reaction conditions, in terms of stirring time and reaction temperature (2), were investigated (Table 2). Subsequently, the solvent was evaporated through vacuum rotary evaporator (Laborota 4000-efficient, Heidolph, Germany) (3). In order to obtain an easy-to-handle powder, the product was rinsed with MilliQ water (4) and filtered with MF-Millipore® 1.2 µm (Sigma-Aldrich, Milan, Italy) in order to remove the uncomplexed NAR (5). Finally, MilliQ water containing NAR/β-CD complex was subjected to freezing at −20°C for 24 hours and subsequent sublimation for 48 hours (NAR/β-CDlyo) (6) (Heto Dryer, Analytica De Mori, Milan, Italy).

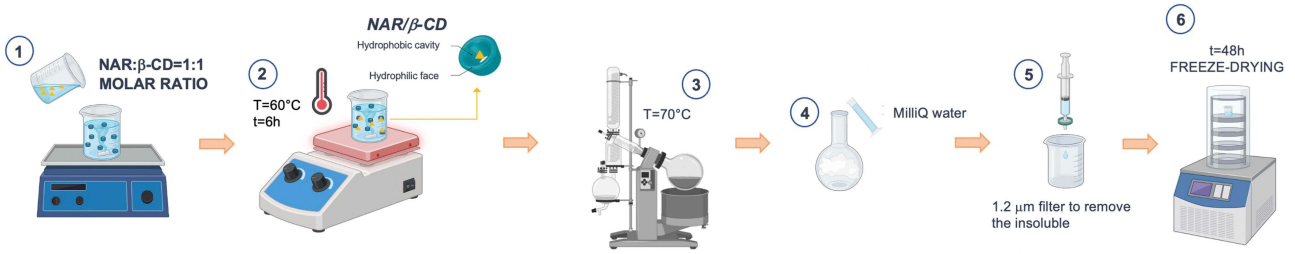

Figure 1 Schematic representation of NAR/β-CD complex preparation: (1) addition of NAR solution to β-CD solution; (2) magnetic stirring of the mixture at 60°C; (3) solvent evaporation through vacuum rotary evaporator; (4) rinsing of the product obtained with MilliQ water and subsequent filtration to remove the uncomplexed NAR (5); (6) freeze-drying of the obtained NAR/β-CD complex.

Characterization of NAR/β-CD Complexes

NAR/β-CD Complexation Efficiency Calculation

The NAR/β-CD complexation efficiency (CE%) was determined by spectrophotometric analysis using a UV-visible spectrophotometer (Perkin Elmer Instruments, Lambda 25, Madrid, Spain): the absorbance of NAR/β-CD solution (obtained after solubilization of a certain NAR/β-CDlyo amount in a known volume of MilliQ water) was measured at 288 nm wavelength, using a quartz cell. In order to quantify the amount of NAR within the NAR/β-CD complex solution, a calibration curve (r^2= 0.9989) was obtained by preparing NAR standard solutions at known and increasing NAR concentrations (0.0025–0.035 mg/mL). Subsequently, the CE% was calculated according to the following equation:

$$CE\,\% = \frac{W_{NARf}}{W_{NAR0}} * 100$$

where W_{NARf} was the amount of NAR within the NAR/β-CD complex and W_{NAR0} was the initial amount of NAR powder used for the complex preparation. All experiments were carried out in triplicate.

Morphological Analysis

The morphology of NAR/β-CDlyo, as well as that of NAR alone, β-CD alone and the physical mixture 1:1 w/w of the two powders (mixNAR_β-CD) as references, was investigated by means of SEM (Phenom™ Pure Desktop, Thermo Scientific, Waltham, Massachusetts, USA). The powders were previously fixed on a stub using double-sided adhesive tape and images were obtained at high voltage, in high vacuum, at room temperature and at a magnification of 2500X.

Table 2 Reaction Conditions Investigated for NAR/-CD Complex Preparation

NAR/β-CD	EtOH	H_2O	EtOH:H_2O (v/v)	T (°C)	Time (h)
1	✓	–	–	25	24
2	✓	–	–	25	24
3	✓	✓	1:4	25	24
4	–	✓	–	25	24
5	✓	✓	1:4	60	0.5
6	✓	✓	1:4	60	1
7	✓	✓	1:4	60	6

https://doi.org/10.2147/IJN.S488507

Water Solubility Evaluation

The water solubility of NAR/β-CD, mixNAR_β-CD and NAR (theoretical NAR amount within NAR/β-CDlyo) was measured after stirring for 24 h at room temperature, throughout UV-visible spectrophotometer in a wavelength range of 220–400 nm (Perkin Elmer Instruments, Lambda 25, Madrid, Spain); β-CD was used as blank.[68,69] After the measurement of the absorbances (A) of each solution at 288 nm, the increase of water solubility % of NAR/β-CD as compared to mixNAR_β-CD and NAR, was respectively calculated according to the following equations:

$$\Delta S\% = \frac{A_{\mathrm{NAR}/\beta-\mathrm{CD}}}{\mathrm{A_{NAR}}} * 100$$

$$\Delta S\% = \frac{A_{\mathrm{NAR}/\beta-\mathrm{CD}}}{A_{\mathrm{mixNAR}\_\beta-CD}} * 100$$

All the experiments were carried out in triplicate.

X-Ray Diffractometry

X-ray diffraction analysis (XRD) on NAR/β-CD, mixNAR_β-CD, β-CD and NAR were carried out on a Cu-anode Bruker AXS D8 instrument working in θ-θ geometry and equipped with a scintillator detector. Scans were performed in the 10–90° range, with a step size 0.02° and a counting time of 8 s/step.

Preparation of lCH/CS Nanogels Loaded with NAR/β-CD Complex

NHs prototypes loaded with NAR/β-CD (NH@NAR/β-CD) were obtained through the same procedure described in section "Preparation of lCH/CS nanogels", previously dissolving the NAR/β-CDlyo into CS solution under magnetic stirring at room temperature, as illustrated in Figure 2.

Characterization of NH@NAR/β-CD Nanogels

Particle Size and Zeta Potential

NHs particle size, polydispersity index (PDI) and zeta potential were investigated by dynamic light scattering (DLS) and electrophoretic light scattering (ELS) (Litesizer 500, Anton Paar, Turin, Italy) as previously reported in section "Particle size and zeta potential".

Encapsulation Efficiency and Loading Capacity Calculation

The encapsulation efficiency of NH@NAR/β-CD was evaluated by centrifugating the NHs dispersion (see section "FITC-dex encapsulation efficiency calculation") and measuring the supernatant absorbance by means of UV-visible spectrophotometer (Perkin Elmer Instruments, Lambda 25, Madrid, Spain) at 288 nm wavelength. A calibration curve was obtained as reported in section "NAR/β-CD complexation efficiency calculation". Once determined the amount of

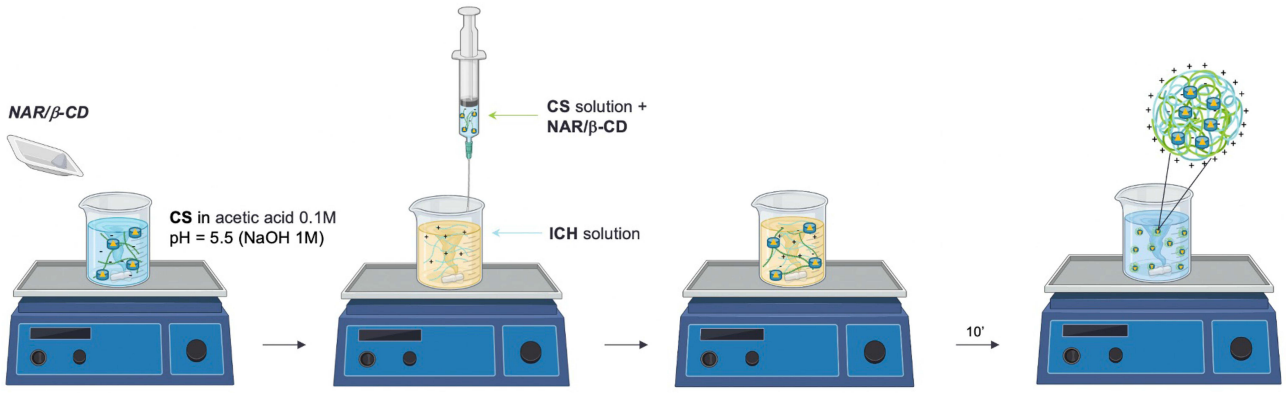

Figure 2 Schematic representation of NH@NAR/β-CD preparation method.

free NAR/β-CD in the supernatant, the EE% and the loading capacity (LC%), were calculated by the following equations:

$$EE\% = \frac{W_{\mathrm{NAR}/\beta-\mathrm{CDlyo}} - W_{\mathrm{freeNAR}/\beta-\mathrm{CD}}}{W_{freeNAR/\beta-CD}} * 100$$

$$LC\% = \frac{W_{\mathrm{NAR}/\beta-\mathrm{CDlyo}} - W_{\mathrm{freeNAR}/\beta-\mathrm{CD}}}{W_{\mathrm{NH@NAR}/\beta-\mathrm{CD}}} * 100$$

where $W_{NAR/\beta-CDlyo}$ was the initial amount of NAR/β-CDlyo added to the NHs preparation, $W_{freeNAR/\beta-CD}$ was the amount of free NAR/β-CD in the supernatant and $W_{NH@NAR/\beta-CD}$ was the total weight of the NHs loaded with the complex. All experiments were carried out in triplicate.

Opacity Determination

In order to investigate the opacity of NHs dispersion after intravitreal injection under in vivo dilution condition, samples were diluted 1:80 v/v[70] in simulated vitreous fluid (SVF) prepared as described by Sapino and co-workers.[71] Briefly, 2 stocks solution of 0.75% w/v hyaluronic acid (HA, 1.7 MDa, Silk-Biomaterial, Italy) and 0.4% w/v agar (Sigma-Aldrich, Italy) were prepared in MilliQ water at 60°C under magnetic stirring. Such solutions were then mixed 1:1 v/v by means of Ultraturrax® T25 easy clean digital (IKA, China) for 5 minutes at room temperature. The opacity of NH@NAR/β-CD was determined from absorbance measurements (A) conducted in a wavelength range of 400–850 nm by means of a spectrophotometer (Perkin Elmer Instruments, Lambda 25, Madrid, Spain) and expressed as transmittance (T%) according to the equation:

$$T\% = e^{-A} * 100$$

The analysis was realized in triplicate.

In vitro NAR Release Test

3 mL of NH@NAR/β-CD was placed in dialysis cassettes (Slide-A-Lyzer™ G3 Dialysis Cassettes, SK MWCO, 3 mL, Thermo Scientific, Milan, Italy) and immersed in 200 mL of SVF (hereafter "dialysis medium"), under magnetic stirring at 37°C for 72 hours. At fixed time endpoints (15 min, 30 min, 1h, 2h, 4h, 8h, 24h, 48, 72h), 3 mL of dialysis medium was collected and replaced with the same volume of fresh SVF, maintained at 37°C. NAR concentration in the dialysis medium was quantified by spectrophotometric method, as previously reported in "NAR/β-CD complexation efficiency calculation". In order to quantify the amount of NAR released, a calibration curve (r^2 = 0.9947) was obtained by preparing NAR standard solutions at known and increasing NAR concentrations (0.005–0.1 mg/mL). For each NHs dispersion, three replicates were prepared and, for each replicate, three measurements were performed.

Antioxidant Properties

NH@NAR/β-CD collected after centrifugation and redispersed in acetate buffer (pH = 5.5), empty NHs dispersion, NAR/β-CDlyo aqueous solution and β-CD aqueous solution were subjected to DPPH assay.[72] Samples were prepared considering the amount of NAR theoretically encapsulated in NH@NAR/β-CD. Each sample was added 1:1 v/v to a DPPH (Sigma-Aldrich, Madrid, Spain) methanol solution (300 μM) and each mixture was kept for 30 minutes in the dark. Mixture absorbance was measured by means of multi-mode microplate reader (FLUOstar Omega Microplate Reader, BMG LabTech, Ortenberg, G) at 517 nm wavelength. NAR ethanol solution diluted 1:1 v/v with DPPH methanol solution and DPPH methanol solution diluted 1:1 v/v with methanol were respectively used as positive and negative controls. Samples not diluted with DPPH methanol solution were used as blanks. The results were expressed as radical scavenging activity percentage (RSA%), as follows:

$$RSA\% = 1 - \frac{A_{\mathrm{sample}} - A_{\mathrm{blank}}}{\mathrm{A_{control}}} * 100$$

 https://doi.org/10.2147/IJN.S488507

where A_{sample} was the absorbance of the sample after 30 minutes of incubation with DPPH methanol solution, A_{blank} was the absorbance of the sample not diluted with DPPH methanol solution and $A_{control}$ was the absorbance of DPPH diluted 1:1 v/v with methanol. Six replicates were performed for each sample.

Cytotoxicity Test

The cytotoxicity of NH@NAR/β-CD, diluted 1:10, 1:25, 1:50 e 1:100 v/v in CM, was assessed on HUVEC cells performing an MTT assay; empty NHs prototypes and NAR/β-CD complex were investigated at the same dilutions and used as references (section "Cytotoxicity test").

Statistical Analysis

Whenever possible, experimental values of the various types of measurements were subjected to statistical analysis, carried out by means of the statistical package GraphPad Prism version 10.1.1. (207) (GraphPad Software, USA). In particular, one-way ANOVA followed by Tukey's multiple comparisons test, Dunnett's multiple comparisons test were carried out; an unpaired *T*-test was also carried out.

Results and Discussion

NHs Preparation and Characterization

The polyelectrolytic complexation represents a safe and environmentally friendly method for producing nano-scale drug delivery systems: it is based on the spontaneous pairing of polyanions and polycations when mixed in aqueous environments, without the need for organic solvents, chemical cross-linkers, or surfactants.[73–75] The use of polysaccharides further contributes to the safety and the sustainability of this method, since they are widely recognized for their lack of toxicity and biodegradability.[76] Several factors play a crucial role in the polyelectrolytic complexation: degree of ionization of each polyelectrolyte, along with their charge density and distribution on polymer chains, concentration and molecular weight (MW) of polyelectrolytes, type of ionic groups on polymer chains, flexibility of polymer chains, ratio and sequence of mixing of polyelectrolytes, time and temperature of interaction, in addition to the pH and the ionic strength of polyelectrolyte solutions.[77,78]

The MW of the polymers involved in the polyelectrolytic complexation could strongly affect both the size and the polydispersity index of the nanoparticles obtained. In particular, shorter polyelectrolyte chains, characterized by higher mobility, tend to produce colloidal dispersion with lower polydispersity, suggesting their ability to form more compact nanostructures.[74,79–81] Additionally, in the present work, a low MW CH was preferred since it was proved that shorter CH chains have a lower tendency of forming intramolecular hydroxyl bonds, leading to a higher availability of activated hydroxyl and amino groups that support the radical scavenging action.[50,51]

It is well known that the pH is responsible for the ionization degree of the polyanions and polycations involved in the formation of the colloidal complexes, especially if weak polyelectrolytes. Therefore, to ensure a proper ionization of their polymer chains and, thus, their subsequent complexation, the pH should be maintained within the range defined by the pKa values of the polyelectrolytes involved.[74,82]

In addition to pH, the polyelectrolyte concentration and the mixing ratio are key factors to allow NHs formation and to avoid their aggregation. In particular, the use of diluted polymeric solutions enhances the formation of NHs that are more evenly distributed in the final colloidal dispersion; in contrast, higher concentrations can lead to polymer chains overlap, resulting in the formation of larger nanoparticles.[83] A polyelectrolyte charge ratio different from 1 permits the production of NHs with a neat surface charge corresponding to the one of the polyion in excess, thus promoting NHs charge repulsion.[77,78]

In the present work, the polyelectrolytic complexation was used to prepare NHs from two stock solutions of lCH and CS. Using the same experimental conditions in terms of stirring speed, time and temperature, the effect of several experimental variables, such as the total polymer concentration ([total polymer]), the polyelectrolyte ratio (lCH:CS ratio) and the pH value of the colloidal dispersion, was investigated on NHs particle size and surface charge. In particular, Figure 3 reports the effect of these variables on the hydrodynamic diameter and the zeta potential of NHs obtained.

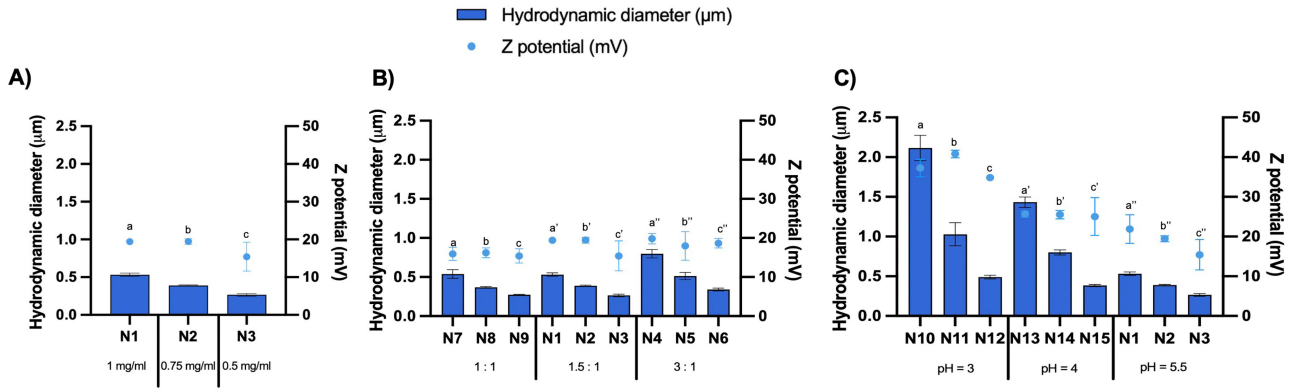

Figure 3 Hydrodynamic diameter and zeta potential values of lCH/CS nanogels (mean value ± s.d.; n=3). ANOVA one-way; MRT (P value ≤ 0.05): (**A**) Hydrodynamic diameter: a vs b,c; b vs c; Zeta potential: a vs c; b vs c. (**B**) Hydrodynamic diameter: a vs a''; a' vs a''; b vs b', b''; b' vs b''; c vs c''; c' vs c''; Zeta potential: a vs a', a''. (**C**) Hydrodynamic diameter: a vs a', a''; a' vs a''; b vs b', b''; b' vs b''; c vs c', c''; c' vs c''; Zeta potential: a vs a', a''; a' vs a''; b vs b', b''; b' vs b''; c vs c', c''; c' vs c''.

In detail, Figures 3A reports the hydrodynamic diameter and the zeta potential of N1-N3, prepared maintaining constant the lCH:CS ratio (1:1.5 (v/v)) and the pH value (5.5), and varying the [total polymer] (1, 0.75, 0.5 mg/mL).[57] It can be observed that a reduction of the [total polymer] leads to a statistically significant decrease of NHs size (from 0.532 μm for N1 to 0.265 μm for N3), suggesting that the presence of fewer polymeric chains could enable their rearrangement and cross-linking into smaller nanostructures. Such results are corroborated by several studies described in the literature concerning the design and the development of chitosan-based nanogels obtained through ionotropic gelation and polyelectrolyte complexation methods.[84–87]

The decrease of the [total polymer] does not result in a consistent variation of the zeta potential values, which remain close to +20 mV. Such result could be explained by the prevalence of the positive charges (protonated amine groups of lCH) over the negative ones (deprotonated sulfonic groups of CS), as expected from the mixing ratio equal to 1:1.5 (v/v).

Figure 3B shows the effect of the experimental variable lCH:CS ratio on the NHs hydrodynamic diameter and zeta potential. Maintaining constant the pH value (5.5), N7-N9 and N4-N6 were prepared at the same [total polymer] used for N1-N3 (1, 0.75, 0.5 mg/mL), though varying the lCH:CS ratios (1:1 (v/v) for N7-N9; 1.5:1 (v/v) for N1-N3; 3:1 (v/v) for N4-N6). The graph highlights that lCH:CS ratios equal to 1.5:1 (v/v) and 1:1 (v/v) are responsible for the production of NHs with smaller hydrodynamic diameter with respect to N4-N6 (3:1 (v/v)); no statistically significant differences occur between N1-N3 and N7-N9 series. The reduction of the hydrodynamic diameters, observed for formulations N7-N9 and N1-N3 in comparison with N4-N6, may be attributed to the difference in the MW between lCH (90–150 kDa) and CS (14 kDa), resulting in a higher abundance of positive charged amine groups compared to negative charged sulfonic groups. Consequently, a higher concentration of lCH (3:1 v/v ratio) at the considered pH value of the colloidal dispersion results in a greater number of positive charges, which produces a higher charge repulsion and, thus, a less densely packed polymeric network.[88] Moreover, all the formulations reported in Figure 3B are characterized by positive zeta potential values (between +15 mV and +20 mV): an abundance of positive charged amino groups with respect to the negative charged sulfonic groups, as provided by lCH:CS ratios equal to 1.5:1 (v/v) or 3:1 (v/v), generates a neat positive charge on NHs surface. As for N7-N9 series, a slight decrease of zeta potential values is probably due to a lCH:CS ratio equal to 1:1 (v/v), that leads to a reduction of the number of the positive charged amino groups with respect to the one of N1-N3 and N4-N6 series; nevertheless, N7-N9 surface charge remains positive as a consequence of the difference in MW between lCH and CS.[88,89]

Finally, Figure 3C shows the hydrodynamic diameter and the zeta potential of N10-N12 and N13-N15, which were prepared at the same [total polymer] used for N1-N3 (1, 0.75, 0.5 mg/mL), maintaining constant lCH:CS ratio (1:1.5 (v/v)), though varying the pH values (pH = 5.5 for N1-N3; pH = 4.0 for N13-N15; pH = 3.0 for N10-N12). The graph highlights the crucial role of the pH on both NHs hydrodynamic diameter and zeta potential, which are both increased as the pH value decreases (up to values of 2.11 μm and +40 mV). As the pH value decreases, the amine groups on lCH chains become increasingly protonated; consequently, the higher density of positive charges on lCH chains leads to a stronger electrostatic

https://doi.org/10.2147/IJN.S488507

Table 3 Hydrodynamic Diameter and Zeta Potential of N3 and N9 Prototypes (mean values ± s.d.; n=3)

Prototypes	[Total Polymer] (mg/mL)	ICH: CS ratio (v/v)	pH	Hydrodynamic Diameter (μm)	Zeta Potential (mV)
N3	0.5	1.5:1	5.5	0.265 ± 0.017	+15.43 ± 3.81
N9	0.5	1:1	5.5	0.275 ± 0.005	+15.43 ± 1.82

repulsion between the chains themselves. Such mutual repulsion prevents the chains from packing closely together, causing the formation of polymer network characterized by a more open structure.[90,91]

In order to allow NHs to reach the retina after intravitreal injection, they should be characterized by a hydrodynamic diameter lower than 350 nm.[35] In addition, nanoparticles with smaller size have been reported to be characterized by an increased residence time after injection. Sakurai et al demonstrated that, after injection of nanospheres with different sizes (2 μm, 200 nm and 50 nm) into the vitreous cavity of pigmented rabbit eyes, the half-life of the nanospheres increased as their size decreased.[92] Moreover, some evidence in the literature reports that NSs presenting a positive surface charge are able to undergo the cellular uptake process: cationic nanoparticles tend to electrostatically interact with the negatively charged plasma membrane and to accumulate within the cells.[93,94] Therefore, after drug loading in NSs, there is an improvement in the drug targeting at the action site and, consequently, an enhancement of the therapeutic efficacy.[32]

According to DLS and ELS results, the best NHs prototypes for the intended purpose of the work, that consists of the development of drug-loaded NHs able to undergo endothelial cellular uptake, are N3 and N9, whose characteristics are reported in Table 3.

Alterations in NHs physico-chemical properties could be correlated to NHs hydrolytic degradation and, thus, could affect NHs behavior during in vitro experiments; in particular, it is well known in the literature that modifications in particle size and surface charge could alter nanoparticle cell uptake.[95] Therefore, a preliminary evaluation of the physico-chemical stability of the two most promising NH prototypes was carried out by monitoring their hydrodynamic diameter, PDI and zeta potential after storage for 7 days at 4°C. Figure 4 reports that no statistically significant differences, in terms of hydrodynamic diameter, PDI and zeta potential, are reported between fresh NHs prototypes (t0) and NHs prototypes after 7 days at 4°C (t7), confirming their storage stability as colloidal dispersion.

The stability of colloidal dispersions relies on nanoparticle surface charge. High zeta potential values guarantee an electrostatic repulsion between nanoparticles, whereas low zeta potential values could lead to aggregation phenomenon.[96] Both N3 and N9 presented positive surface charge and the resulting values are close to those reported for CH nanoparticles realized by Ribeiro and co-workers and for CH and sodium tripolyphosphate nanoparticles of Pereira et al[97,98] Additionally, the stability of colloidal dispersions can be strongly influenced by the presence of structural hydration layers formed by water

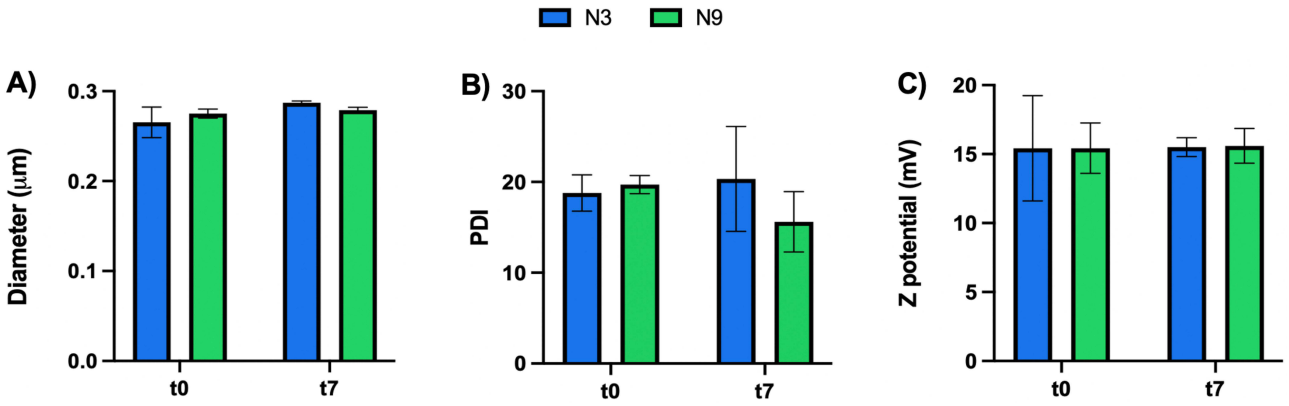

Figure 4 Hydrodynamic diameter (**A**) PDI (**B**) and zeta potential (**C**) values at t0 and t7 days of N3 and N9 prototypes (mean value ± s.d.; n=3). ANOVA one-way; *T* test ($p < 0.05$).

molecules on the NHs surfaces. These hydration layers could avoid aggregation phenomena through two mechanisms: steric hindrance, which physically prevents close interactions between nanoparticles, and electrostatic repulsion, which alters surface charge distribution.[99]

NTA was used to determine number-weighted sizes and concentrations of the two most promising NHs prototypes. The concentrations of N3 and N9 were equal to 2.17×10^{12} and 9.32×10^{10} respectively (Figure 5); such difference (amounting to two orders of magnitude) suggested that, although N3 and N9 protypes contained the same [total polymer] and were characterized by the same pH value, the optimal lCH:CS ratio for NHs preparation was 1.5:1 (v/v), namely the condition at which there was a neat surface charge corresponding to the one of the polyion in excess.[77,78]

Moreover, NTA revealed that the 98.89% of NHs constituting N3 prototype were characterized by a hydrodynamic diameter lower than 350 nm, whereas for N9 prototype this fraction was equal to 74.90% (Figure 5).

As for N9 prototype, it can be noticed that the hydrodynamic diameter values determined by DLS analysis and NTA were almost superimposable (approximately 0.275 µm for DLS and 0.286 µm with NTA); on the contrary, for N3 prototype, the results obtained with the two techniques were consistently different (approximately 0.265 µm for DLS and 0.111 µm with NTA). The observed discrepancy between DLS and NTA results could be attributed to the different sample dilution and the detection principles of the two techniques. NTA required a significant sample dilution (1:10,000 for N3 and 1:1000 for N9 in acetate buffer, pH = 5.5), whereas DLS was performed on the sample as such. During DLS analysis, the presence of particles with larger size or higher particle concentrations could hinder an accurate size determination of the population of smaller particles leading to an overestimation of the average hydrodynamic diameter, such in the case of N3. Conversely, NTA tracks and sizes individual particles in a diluted sample, reducing the influence of high scattering intensities from larger particles. At the lower concentration of N9 (10^{10} particles/mL), the scattering events in DLS are less dominated by larger particles, resulting in size more consistent with NTA.[100] In a recent work, McComiskey et al reported the same discrepancy between DLS and NTA measurements for azole anti-fungal nano-dispersions.[101]

Videos S1 and S2, presenting the visualization of both N3 and N9 prototypes at the dilutions of 1:10,000 and 1:1000 respectively, are provided. Such videos allow a comprehensive observation of nanoparticle behavior when dispersed in an aqueous medium, also in terms of dynamic tracking and size distribution.

Figure 6 shows SEM images (A), obtained upon NHs freeze-drying, and TEM micrographs (B), acquired after NHs dilution 1:100 v/v in acetate buffer (pH = 5.5) and subsequent staining with phosphotungstic acid, of N3 and N9. In Figure 6A, it can be observed that both prototypes are characterized by a non-completely spherical shape and

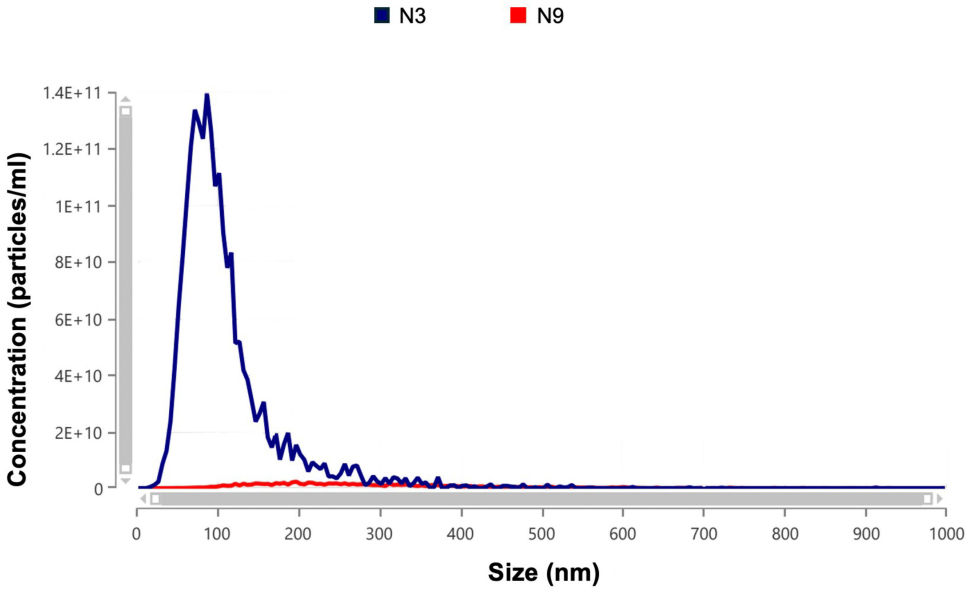

Figure 5 Average size distribution of N3 (dil 1:10,000) and N9 (dil 1:1,000) prototypes.

https://doi.org/10.2147/IJN.S488507

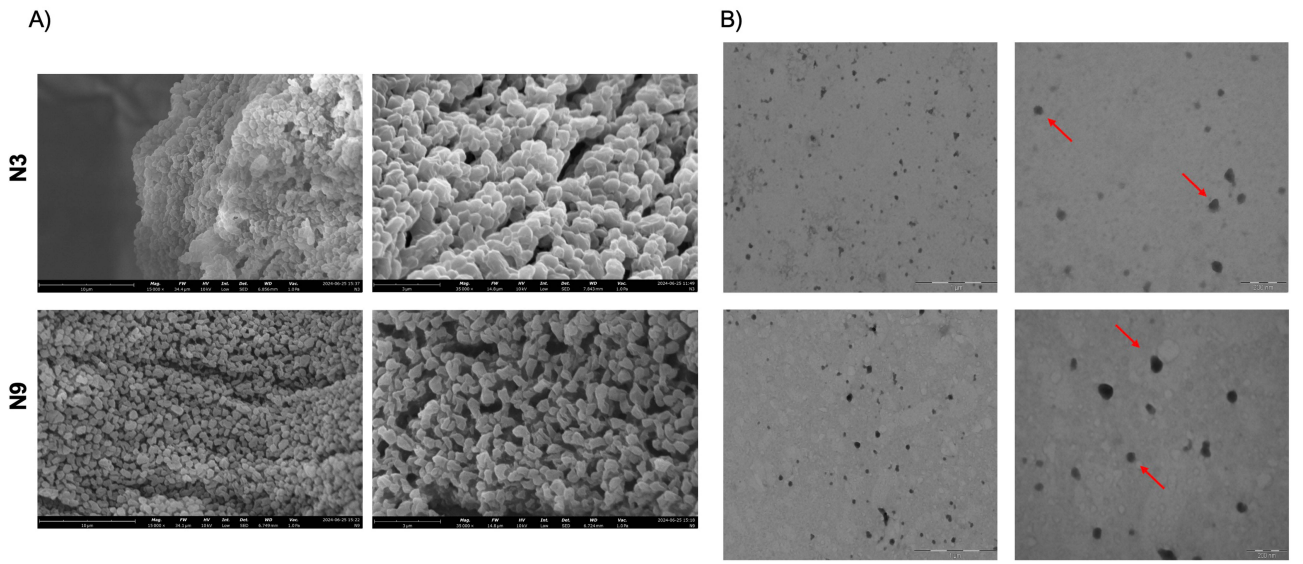

Figure 6 SEM images (**A**) at two different magnifications (10.0 kX and 20.0 kX) of freeze-dried prototypes N3 and N9; TEM micrographs (**B**) at two different magnifications (50 kX and 100 kX) of evaporated prototypes N3 and N9 diluted 1:100 and stained with phosphotungstic acid for 1 minute.

a heterogeneous morphology, probably due to NHs aggregation during freeze-drying. Such results were confirmed by the literature: Feyzioglu and Tornuk reported the same aggregation phenomenon for CH-based nanoparticles, as well as Waiprib and coworkers for CS/CH nanoparticles.[102,103] In Figure 6B, it is shown that the two NHs prototypes were nearly spherical with a more homogeneous morphology. The difference between TEM and SEM images could be explained by the different sample preparation methods used (NHs freeze-drying as such for SEM; NHs dilution 1:100 v/v and drying for TEM), in accordance with other evidence reported in the literature.[91,104] Moreover, the NHs prototypes dimensions measured on SEM and TEM images (70–100 nm; ImageJ™ software) are smaller than the mean hydrodynamic diameter determined by DLS. This behavior could be explained since during DLS analysis, NHs were dispersed in an aqueous medium and, thus, in swollen state, instead for SEM/TEM analysis NHs were analyzed in dry state; the absence of the solvent from NHs dispersion results in a reduction of the mean diameter. Similar observations were reported in the works of Valentino et al concerning the development of alginate-spermidine NHs, and Esmaeili and Asgari, who produced chitosan nanoparticles.[60,105]

Cytotoxicity effect and cellular uptake of N3 and N9 prototypes were evaluated on endothelial cells. Indeed, DR is primarily a microvascular disease, and endothelial dysfunctions may even precede neurodegeneration.[106] Specifically, HUVEC cells are extensively employed as a cellular model in retina research to explore various aspects ranging from angiogenesis to degeneration.[107,108] Moreover, HUVEC cells are a fully characterized cellular model, exhibiting the same marker expression as the retinal microvascular endothelial cells and responsiveness to VEGF and other growth factors. In addition, HUVEC seem better suited for establishing models intended for long-term studies, while commercially available retinal endothelial cells maintain their phenotype for only a few passages.[109,110]

Results of the toxicity test are reported in Figure 7 as the percentage of the cell mitochondrial activity, evaluated through MTT assay after 24 hours of cell contact with different dilutions of NHs in CM. In the adopted experimental conditions, both N3 and N9 prototypes were biocompatible at all the tested concentrations since characterized by mitochondrial activity % values not statistically different from that observed for CM. Indeed, a tested product is considered to have a cytotoxic potential only when the cell viability decreases below 70% in comparison to the control group.[111] As regarding to N3, a kind of bell-shape dose-response curve can be observed, with an increase in mitochondrial activity % after dilution 1:25 v/v in CM; this profile is not uncommon when testing the effect of colloidal drug formulation on biological substrates.[112,113]

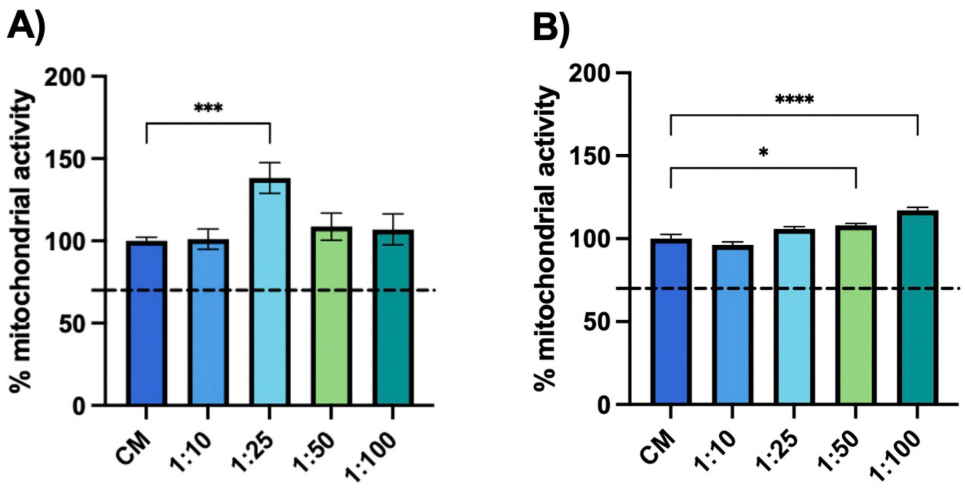

Figure 7 Mitochondrial activity % values calculated for N3 (**A**) and N9 (**B**) prototypes after dilution 1:10, 1:25, 1:50, 1:100 v/v in CM. CM was used as reference (mean values ± s.d.; n = 6). ANOVA one-way; Dunnett's test ($p < 0.05$).

Considering NTA results that highlight a higher NHs concentration for N3 and its proved biocompatibility, N3 was selected as the best NH prototype to be further characterized.

In particular, the capability of N3 to be internalized into HUVEC cells was appreciated throughout CLSM analysis. For this purpose, N3 prototype was loaded with FITC-dex as fluorescent probe and the EE% of NH@FITC-dex was calculated, resulting equal to 67.67%.

Before testing, NHs prototypes stability upon dilution in CM was assessed (Supplementary data; Figure 1S).

Figure 8 shows CLSM images of untreated cells (A) as compared to those put in contact for 3 hours with NH@FITC-dex at a dilution of 1:25 v/v in CM (B). Figure 8B highlights the presence of NHs (marked in green) within the cell cytoskeleton (marked in red), confirmed also by the orthogonal projection view and Z-stack images (Supplementary data; Figure 2S); no green fluorescence is observed in the untreated cells image (A). Such results suggest that N3 prototype

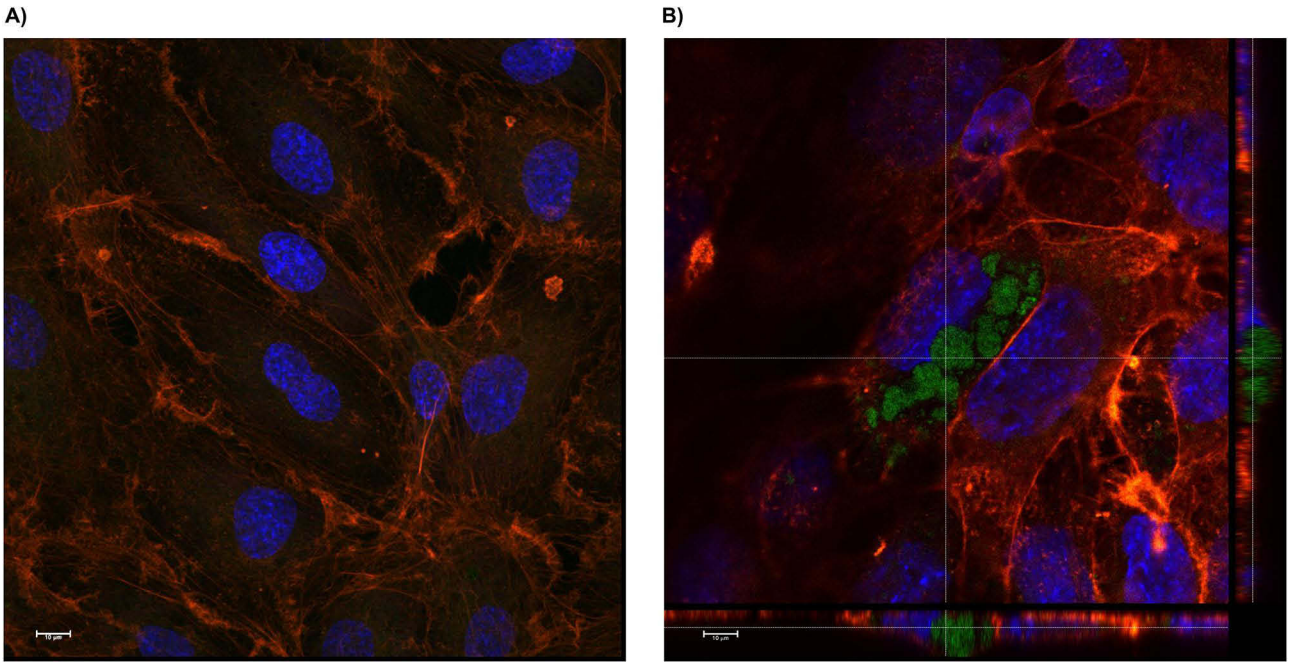

Figure 8 HUVEC cellular uptake studies by means of confocal microscopy on N3 diluted 1:25 v/v (**B**) as compared to the untreated control (**A**). Green: FITC-dex (λ_{ex}= 490 nm) loaded into N3; blue: Hoechst dye (λ_{ex}= 361 nm/ λ_{em}= 497 nm) specific for nuclei staining; red: TRITC (λ_{ex}= 514 nm and λ_{em}= 580 nm) for actin fibers staining.

https://doi.org/10.2147/IJN.S488507

Table 4 CE% Values of Each Experimental Set Up of NAR/β-CD Preparation (mean value ± s.d.)

Sample	Time (h)	T (°C)	CE%
NAR/β-CD 1	24	25	25.20
NAR/β-CD 2	24	25	8.26
NAR/β-CD 3	24	25	19.00
NAR/β-CD 4	24	25	15.11
NAR/β-CD 5	0.5	60	28.80
NAR/β-CD 6	1	60	33.71
NAR/β-CD 7	6	60	71.13

shows the capability to be internalized into HUVEC cells and, thus, should allow the direct targeting of retinal endothelial cells.

Preparation and Characterization of NAR/β-CD Complex

NAR/β-CD complex was prepared according to the co-precipitation method, one of the most simple and efficient method used for the preparation of inclusion complexes between CDs and water insoluble active molecules.[110] Such complex is intended to be loaded into NHs prototype due to its antioxidant properties useful in the treatment of the early stages of DR.

Two reaction conditions, namely reaction time and temperature, were investigated and, for each experimental set up, CE% was calculated after spectrophotometric analysis. The results reported in Table 4 show that the NAR/β-CD complex formation was favored at 60°C in respect to 25°C. CE% value, obtained after 6 h of reaction at 60°C, is similar to those reported in the work of Semalty and co-workers, which prepared inclusion complexes between NAR and β-CD;[114] moreover, an increase of CE% value was associated with an increase in the reaction time, as observed in other studies.[115,116]

Figure 9 shows the SEM micrographs of NAR/β-CDlyo (A) and mixNAR_β-CD (B) (namely NAR/β-CD after the freeze-drying process and physical mixture of NAR and β-CD); NAR (C) and β-CD (D) are used as references. In particular, NAR and β-CD powders are characterized by a well defined morphology; NAR shows a needle shape, while β-CD appears in the form of compact blocks with an uneven and irregular surface (Figure 9C and D). In Figure 9B, for mixNAR_ β-CD, it is possible to observe the coexistence of both specimens with unchanged morphologies; in Figure 9A, it is possible to appreciate a compact and homogeneous plate-like structure, quite different from the sizes and shapes of NAR and β-CD (Figure 9C and D), which confirms the formation of NAR/β-CD complex. These differences in morphology and dimensions are similar to those reported in the works of Semalty et al and Yang and co-workers for NAR, β-CD, their physical mixture and complex and could be considered as a proof of the occurred complexation.[69,114]

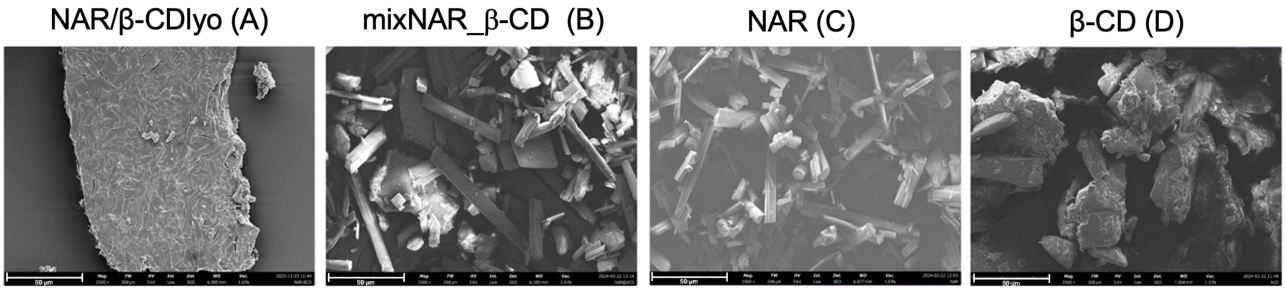

Figure 9 SEM images at magnification of 2500 X of NAR/β-CDlyo (**A**) and NAR@β-CD (**B**), NAR (**C**), β-CD (**D**).

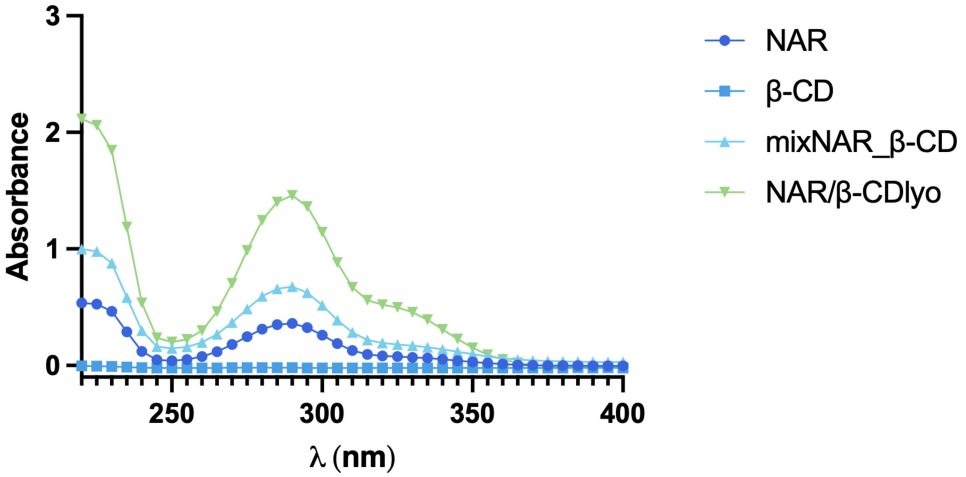

Figure 10 Absorption spectra in the range of 220–400 nm of NAR/β-CDlyo, mixNAR_β-CD, NAR, and β-CD.

In order to prove the increase of NAR water solubility when complexed with β-CD, a quantitative investigation of the water solubility of NAR/β-CDlyo as compared to NAR and mixNAR_β-CD was carried out by a spectrophotometric method.

As illustrated in Figure 10, NAR, mixNAR_β-CD and NAR/β-CDlyo present the characteristic absorption peaks of NAR at 288 nm; as expected, the NAR aqueous solution shows the lowest absorbance curve, suggesting that a small amount of NAR dissolves in water. An addition of β-CD leads to an enhancement of the NAR dissolution in water and, consequentially, of the NAR absorbance profile, equal to 87.78% as compared to NAR; the highest absorbance value is associated with the NAR/β-CDlyo solution, which confers an improvement of NAR water solubility of 305.44% in comparison with NAR, and of 115.91% with mixNAR_β-CD. Such results could be explained since the formation of the inclusion complex that occurs in water, which is responsible for the increase in NAR water solubility, is based on a dynamic equilibrium between the complexed form NAR/β-CD and the free species NAR and β-CD; the main driving forces of this dynamic equilibrium are reported to be release of enthalpy-rich water molecules from the cavity and hydrophobic interactions.[114,117] Once the NAR molecules are added to a β-CD solution, the reaction takes place and a small amount of NAR molecules complexes with β-CD molecules, thus explaining the NAR water solubility increase also in the mixNAR_β-CD. This enhancement in the NAR water solubility in the physical mixture mixNAR_β-CD is confirmed by the work of Sadaquat and Akhtar on β-CD and docetaxel, and by the work of Wen et al on NAR and Hydroxypropyl β-CD.[67,118] As the temperature and the reaction time increase, the dynamic equilibrium is shift to the formation of the NAR/β-CD complex. Such increase is confirmed by several studies, which demonstrated that the formation of inclusion complexes between β-CD and lipophilic drugs was responsible for an enhancement in their water solubility.[114,119,120]

This strategy results thus suitable for NAR loading in N3 prototype previously developed; other previously studies reported in literature related with CH nanoparticles exploit the formation of inclusion complexes with β-CD for hydrophobic drug delivery.[121–123]

The powder X-ray diffraction (XRD) patterns of NAR, β-CD, mixNAR_β-CD and NAR/β-CD are shown in Figure 11. In particular, sharp diffraction peaks indicated the high crystallinity of NAR and β-CD. The XRD pattern of mixNAR_β-CD (namely physical mixture of NAR and β-CD) was similar with those of pure materials as a sum of the two patterns. On the other hand, the diffraction pattern obtained from the NAR/β-CD showed a relevant decrease in the number and intensity of diffraction peaks compared with pure β-CD and pure NAR, suggesting an amorphous structure. XRD results explained the enhanced solubility of NAR/β-CD as compared to NAR alone: it is well known that the amorphous state is markedly more soluble than the crystalline counterpart.[124] This result pointed out that the crystalline structure of the NAR/β-CD complex was different from that of the pure materials, confirming the formation of the inclusion complex. The results obtained are in line with those reported in the literature.[125,126]

https://doi.org/10.2147/IJN.S488507

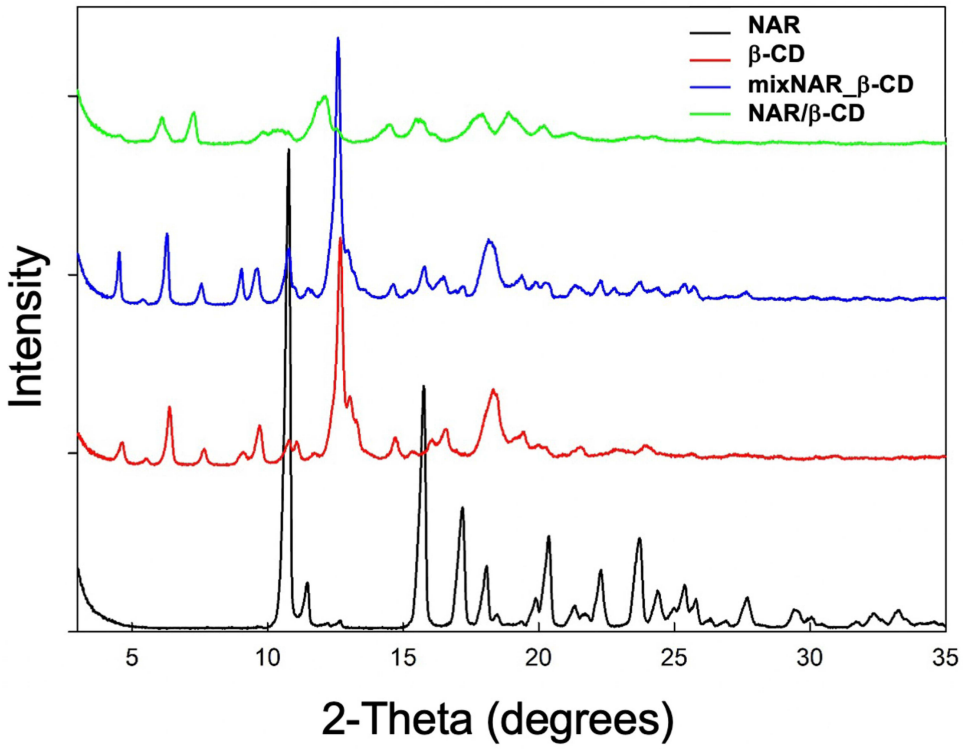

Figure 11 Diffraction patterns of NAR/β-CD and references NAR, β-CD, mixNAR_β-CD.

Preparation and Characterization of NH@NAR/ β -CD Nanogels

NAR/β-CDlyo was solubilized in CS solution and then added to lCH solution as previously reported for the polyelectrolyte complexation method. N3@NAR/β-CD was characterized in terms of hydrodynamic diameter and zeta potential; such values were compared to those obtained for empty N3 to highlight any changes in the dimensional and surface characteristics, which could be attributable to the encapsulation of NAR/β-CD. No statistically significant differences were observed between N3 and N3@NAR/β-CD in terms of hydrodynamic diameter (0.265 ± 0.001 μm for N3 vs 0.273 ± 0.008 μm for N3@NAR/β-CD), meaning that the loading of the complex did not affect NHs particle size. Regarding the surface charge, instead, N3@NAR/β-CD was characterized by a statistically significant higher zeta potential value than N3 (from + 15.43 ± 3.81 mV to + 19.36 ± 0.27 mV). Hence, given the positive charge of N3@NAR/β-CD, NHs cellular uptake and storage stability could be considered equal to those of empty N3.

N3@NAR/β-CD was also characterized in terms of EE% and LC%, resulting equal to 81.80 ± 1.23% and 27.20 ± 0.89%, respectively, confirming the NAR/β-CD encapsulation.

In order to avoid visual perturbations after colloid intravitreal injection, the opacity of the NHs dispersion was evaluated.[127,128] Before spectrophotometric analysis, N3@NAR/β-CD was diluted 1:80 v/v with SVF; such dilution was selected considering that the vitreous body volume was equal to 4 mL and 50–100 μL is the most appropriate volume range to be injected in order to avoid intraocular pressure.[70] N3@NAR/β-CD was characterised by T% values higher than 98% in the whole wavelength range investigated (400–850 nm), thus confirming its suitability to be injected into the vitreous body.

Figure 12 reports the % NAR released from N3 when placed in contact for 72 hours with SVF. According to the results reported in the graph, N3 released about 75% of NAR within 72 hours; such result confirms the N3@NAR/β-CD capability to sustain in vitro NAR release.

The high susceptibility of the retina to oxidative stress and its role in the onset and progression of DR has been widely investigated by different research groups. Wu et al and Rossino and Casini highlighted that the oxidative stress initiates a self-propagating phenomenon, leading to a continuous rise in ROS levels; this persistent increase in ROS subsequently

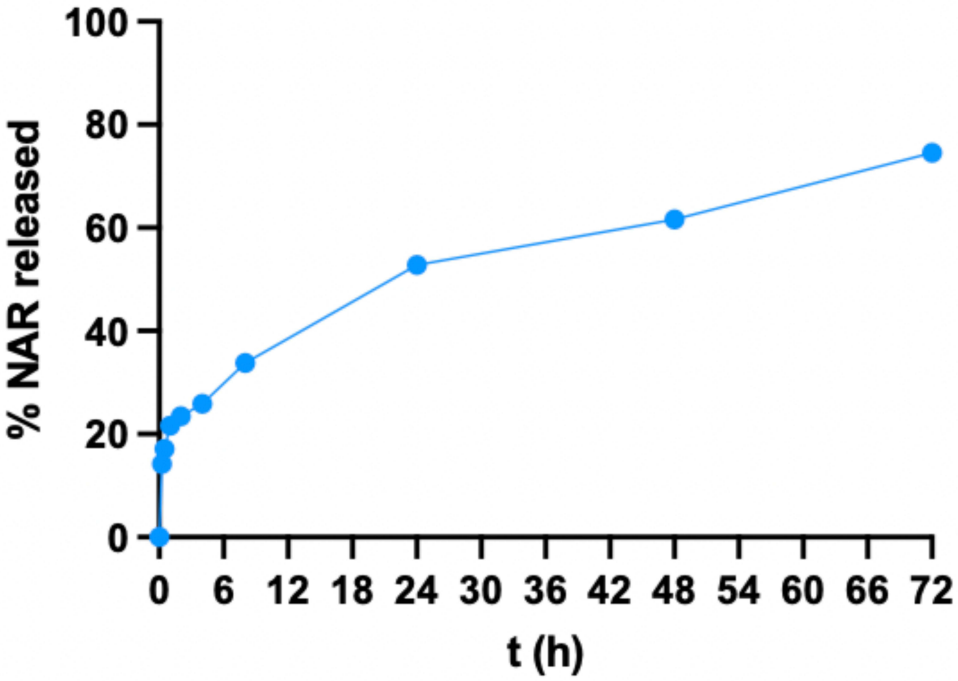

Figure 12 NAR release profiles from N3@NAR/β-CD (mean values ± s.d.; n = 3; CV <12%).

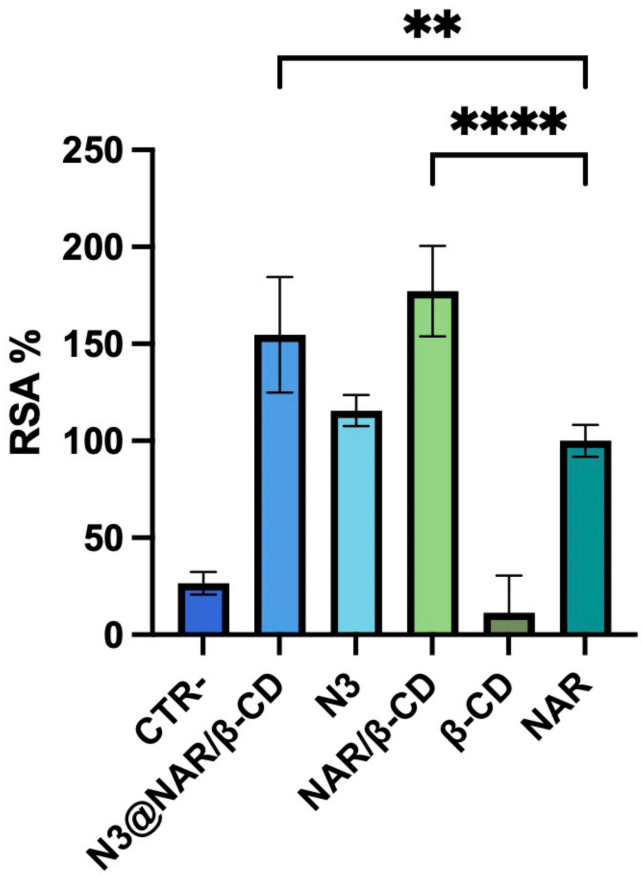

Figure 13 RSA% of N3@NAR/β-CD, N3, NAR/β-CD and β-CD. CTR- and NAR are considered as negative and positive controls respectively (mean values ± s.d.; n = 3). ANOVA one-way; Dunnett's test ($p < 0.05$).

https://doi.org/10.2147/IJN.S488507

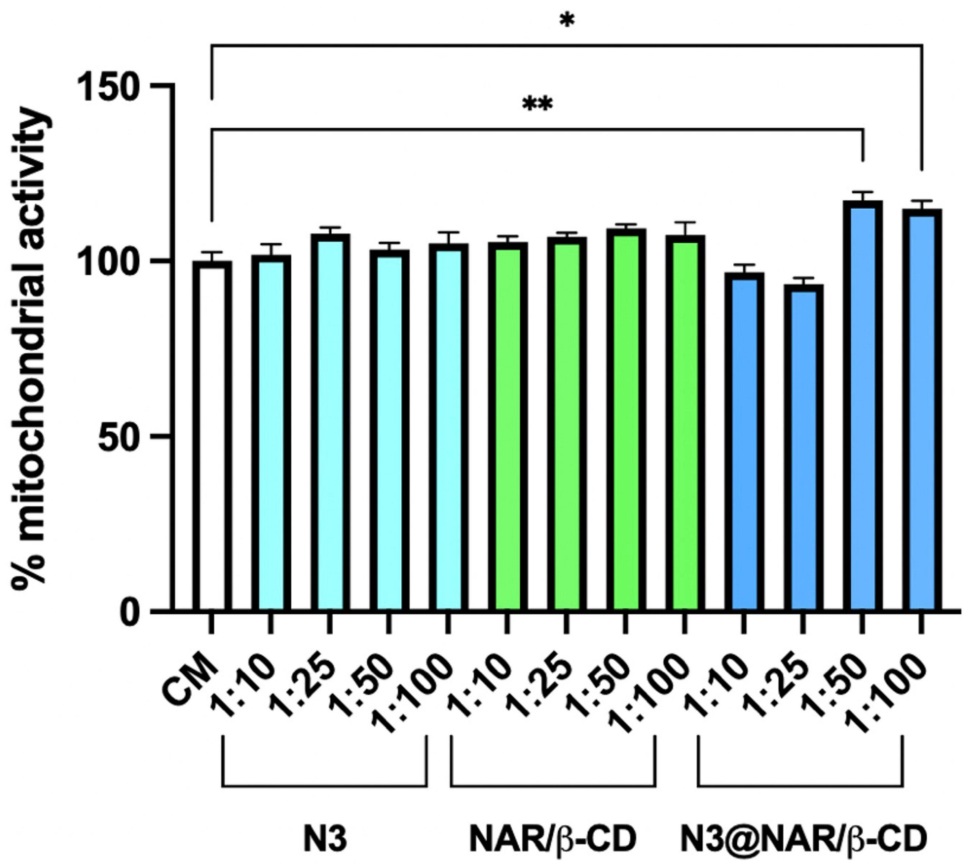

Figure 14 Mitochondrial activity % values calculated for N3, NAR/β-CD and N3@NAR/β-CD diluted 1:10, 1:25, 1:50, 1:100 v/v in CM. CM was used as reference (mean values ± s.d.; n = 6). ANOVA one-way; Dunnett's test ($p < 0.05$).

activates pathways that are strictly associated with the progression of DR.[129,130] NAR is known in the literature as capable to attenuate oxidative stress and cell apoptosis and to improve neurotrophic effects in diabetic retina;[131] its antioxidant property, when complexed with β-CD and loaded into N3, was investigated throughout a DPPH assay, assessing the N3@NAR/β-CD capacity to lower DPPH, a standard nitrogen-concentrated free radical. Chiang and his team have shown that some compounds (ie fucoxanthin), demonstrated to be endowed with a radical scavenging activity by a DPPH assay, exhibited significant antioxidant properties by effectively reducing oxidative stress and preventing cellular damage in DR cellular models. In the work of Chiang et al, ARPE-19 retinal cells were exposed to high glucose levels and then treated with fucoxanthin, which effectively decreased ROS levels, enhanced catalase activity, and preserved retinal cell integrity. These in vitro results suggested that DPPH assay may be useful as a reliable preliminary method to predict the clinical efficacy of antioxidant treatment in DR.[132]

Figure 13 shows the antioxidant properties, expressed as RSA%, of N3@NAR/β-CD, N3, NAR/β-CD ad β-CD as compared to those of the negative control (DPPH alone, CTR-) and the positive control (NAR). The graph shows that N3@NAR/β-CD and NAR/β-CD have a statistically significant higher antioxidant potential than NAR. These results could be explained since the inclusion complex with β-CD is responsible for a higher NAR solubility in water, allowing a better interaction of NAR with free radicals.[133,134] Similar outcomes were described by Liu et al in which increased radical scavenging activity was detected for ovalbumin and curcumin complexed with CDs, as compared to their uncomplex forms.[135] In addition, RSA% value of N3 is comparable with that of NAR, confirming the antioxidant behaviour of both lCH and CS.

Finally, cell viability after treatment with N3@NAR/β-CD was assessed in vitro on HUVEC cells and compared with the results obtained for NAR/β-CD and empty N3. Results are reported in Figure 14 as the percentage of the cell mitochondrial activity, evaluated with MTT assay after 24 hours of cell contact with different dilutions of the three

samples in CM. For the mitochondrial activity % values of N3@NAR/β-CD, NAR/β-CD and N3 at all the dilutions considered, no statistically significant differences with CM are reported, meaning that all the samples can be considered biocompatible; additionally, the dilutions 1:50 and 1:100 of N3@NAR/β-CD in CM are characterized by a mitochondrial activity % values statistically higher than the CM. Such result could be explained since it is reported in the literature that, for CH NSs, a lower charge density of the particles is responsible for a higher cell viability; therefore, a higher dilution of 1:50 and 1:100 of N3@NAR/β-CD as compared to the others, lower the charge density of the system resulting in higher mitochondrial activity % values.[136]

N3@NAR/β-CD exhibited a size lower than 350 nm and a positive zeta potential. Such physico-chemical properties were responsible for NHs cell uptake, suggesting their potential to target retinal endothelial cells and, consequently, to enhance therapeutic efficacy. Furthermore, the high complexation efficiency of approximately 82% and the sustained release of NAR/β-CD over 72 hours could guarantee the maintenance of an effective drug concentration at the site of action while reducing the need for frequent injections. All the above-mentioned properties could overcome current limitations in retinal drug delivery, providing a promising approach for targeting endothelial cells in DR.

Conclusion

In the first phase of the present work, an optimized prototype of NHs based on natural biopolymers endowed with antioxidant properties, namely chitosan and chondroitin sulphate, was successfully developed using the polyelectrolyte complexation method; total polymer concentration, lCH:CS ratio and pH were systematically varied to identify the optimal experimental conditions to obtain NHs characterized by size and surface charge proper for the intended use. Particle size measurements revealed that lower total polymer concentrations and higher pH values led to the production of NHs characterized by smaller dimension. Zeta potential measurements indicated that NHs with higher pH values exhibited adequate positive zeta potentials, suggesting enhanced physical stability over time and higher potential for cellular interactions and uptake. Among the colloidal dispersions tested, N3 and N9, both prepared at pH 5.5 with a total polymer concentration of 0.5 mg/mL and differing for lCH:CS ratio (1.5:1 for N3 and 1:1 for N9), emerged as the most promising NHs prototypes. These prototypes exhibited suitable hydrodynamic diameters (<350 nm) and zeta potential values (approximately +15 mV) to provide endothelial cells internalization; in addition, high zeta potential values ensure that the prototypes remained stable throughout the tested storage period. N3 demonstrated narrower particle size distribution and higher number of NHs compared to N9, as evidenced by NTA results. In vitro cytotoxicity tests using HUVEC as cell model confirmed that N3 was well tolerated and CLSM analyses demonstrated its capability to be efficient internalized, highlighting its potential to be used as versatile systems for the delivery of drugs or bioactive molecules.

The second phase of the work included the production of an inclusion complex (NAR/β-CD) between NAR and β-CD to enhance the solubility of NAR. The complexation efficiency of NAR/β-CD was optimized under specific reaction conditions, resulting in significant improvements in water solubility, compared to free NAR. In addition, XRD pattern of NAR/β-CD confirmed the inclusion complex formation, after comparison with those of NAR and β-CD.

Finally, the encapsulation of the NAR/β-CD complex into N3 prototype (N3@NAR/β-CD) did not significantly impact the particle size but increased the zeta potential, suggesting improved cellular uptake and storage stability. The high encapsulation efficiency (EE%) and loading capacity (LC%) confirmed the effective incorporation of the NAR/β-CD complex. Moreover, the high transparency of N3@NAR/β-CD indicates its suitability for intravitreal injections without causing visual disturbances. The in vitro release study pointed out that N3 prototype succeeded to sustain NAR/β-CD complex over 72 hours. In vitro DPPH assay confirmed that empty N3 exerted an antioxidant activity due to the intrinsic biological properties of the constituting polymers (lCH and CS), and N3@NAR/β-CD was effective in reducing oxidative stress, a critical factor in the progression of DR. Furthermore, in vitro cell viability assays confirmed the biocompatibility of N3@NAR/β-CD at various dilutions. These results collectively suggest that N3@NAR/β-CD represents a promising candidate to be further explored as a potential treatment for counteracting the effect of oxidative stress in the development of DR, with a particular focus on the early stages of the disease. In order to assure a long-term stability of NHs, future studies will be focused on the freeze-drying of the NHs dispersion developed in the present work; the addition of cryoprotectants will be considered to produce freeze-dried NHs readily redispersible upon reconstitution

with saline (before intravitreal injection). Further studies will be carried out to deeply explore the effects of NHs@NAR/β-CD on key molecular pathways closely associated with the disease, both in vitro and in vivo using animal models.

Acknowledgments

The authors would like to thank Dr. Massimo Boiocchi (Centro Grandi Strumenti, University of Pavia) for his assistance in TEM analyses, Dr. Patrizia Vaghi and Dr. Amanda Oldani (Centro Grandi Strumenti, University of Pavia) for their kind support in CLSM analyses and Dr. Roberto Santoliquido for Nanoparticle tracking analysis. This study was partially supported by a grant to AP from MIUR, PRIN 2020 (2020FR7TCL_003).

Author Contributions

All authors made a significant contribution to the work reported, whether that is in the conception, study design, execution, acquisition of data, analysis and interpretation, or in all these areas; took part in drafting, revising or critically reviewing the article; gave final approval of the version to be published; have agreed on the journal to which the article has been submitted; and agree to be accountable for all aspects of the work. GZ, BV and SR conceived and designed the experiments and wrote the paper. GZ, CV, GG and NM performed the experiments and acquired experimental data. GZ, BV, LM, AP and SR analyzed and interpreted the experimental data. BV, MR, GS and SR revised the article.

Disclosure

The authors declare that they have no known competing financial interests or personal relationships that could have appeared to influence the work reported in this work.

References

1. Diabetes: health topics of the world health organization. Available from: https://www.who.int/health-topics/diabetes#tab=tab_1. Accessed January 8, 2024.
2. Wong TY, Cheung CMG, Larsen M, Sharma S, Simò R. Diabetic retinopathy. *Nat Rev Dis Primers*. 2016;2(1):16012. doi:10.1038/nrdp.2016.12
3. Beli E, Yan Y, Moldovan L, et al. Restructuring of the gut microbiome by intermittent fasting prevents retinopathy and prolongs survival in db/db mice. *Diabetes*. 2018;67(9):1867–1879. doi:10.2337/db18-0158
4. Kang Q, Yang C. Oxidative stress and diabetic retinopathy: molecular mechanisms, pathogenetic role and therapeutic implications. *Redox Biol*. 2020;37:101799. doi:10.1016/j.redox.2020.101799
5. Ajlan RS, Silva PS, Sun JK. Vascular endothelial growth factor and diabetic retinal disease. *Semin Ophthalmol*. 2016;31(1–2):40–48. doi:10.3109/08820538.2015.1114833
6. Antonetti DA, Silva PS, Stitt AW. Current understanding of the molecular and cellular pathology of diabetic retinopathy. *Nat Rev Endocrinol*. 2021;17(4):195–206. doi:10.1038/s41574-020-00451-4
7. Kropp M, Golubnitschaja O, Mazurakova A, et al. Diabetic retinopathy as the leading cause of blindness and early predictor of cascading complications-risks and mitigation. *EPMA J*. 2023;14(1):21–42. doi:10.1007/s13167-023-00314-8
8. Giri B, Dey S, Das T, Sarkar M, Banerjee J, Dash SK. Chronic hyperglycemia mediated physiological alteration and metabolic distortion leads to organ dysfunction, infection, cancer progression and other pathophysiological consequences: an update on glucose toxicity. *Biomed Pharmacother*. 2018;107:306–328. doi:10.1016/j.biopha.2018.07.157
9. Hammes HP. Diabetic retinopathy: hyperglycaemia, oxidative stress and beyond. *Diabetologia*. 2018;61(1):29–38. doi:10.1007/s00125-017-4435-8
10. Annadurai T, Thomas PA, Geraldine P. Ameliorative effect of naringenin on hyperglycemia-mediated inflammation in hepatic and pancreatic tissues of Wistar rats with streptozotocin- nicotinamide-induced experimental diabetes mellitus. *Free Radic Res*. 2013;47(10):793–803. doi:10.3109/10715762.2013.823643
11. Venkateswara Rao P, Kiran SDVS, Rohini P, Bhagyasree P. Flavonoid: a review on Naringenin. *J Pharmacogn Phytochem*. 2017;6(5):2778–2783.
12. Bhia M, Motallebi M, Abadi B, et al. Naringenin nano-delivery systems and their therapeutic applications. *Pharmaceutics*. 2021;13(2):291. doi:10.3390/pharmaceutics13020291
13. Al-Dosari DI, Ahmed MM, Al-Rejaie SS, Alhomida AS, Ola MS. Flavonoid naringenin attenuates oxidative stress, apoptosis and improves neurotrophic effects in the diabetic rat retina. *Nutrients*. 2017;9(10):1161. doi:10.3390/nu9101161
14. Wang Y, Jiao Y, Chun C, Yingjuan H. Effects of naringenin on oxidative damage and cell apoptosis in diabetic retinopathy rats via the Nrf2/ARE signaling pathway. *Indian J Pharm Sci*. 2021;83(5):899–905. doi:10.36468/pharmaceutical-sciences.841
15. Ola MS, Nawaz MI, Siddiquei MM, Al-Amro S, El-Asrar AMA. Recent advances in understanding the biochemical and molecular mechanism of diabetic retinopathy. *JDC*. 2012;26(1):56–64.
16. Payne AJ, Kaja S, Naumchuk Y, Kunjukunju N, Koulen P. Antioxidant drug therapy approaches for neuroprotection in chronic diseases of the retina. *Int J Mol Sci*. 2014;15(2):1865–1886. doi:10.3390/ijms15021865
17. Rahigude A, Bhutada P, Kaulaskar S, Aswar M, Otari K. Participation of antioxidant and cholinergic system in protective effect of naringenin against type-2 diabetes-induced memory dysfunction in rats. *Neuroscience*. 2012;226:62–72. doi:10.1016/j.neuroscience.2012.09.026

18. Roy S, Ahmed F, Banerjee S, Saha U. Naringenin ameliorates streptozotocin-induced diabetic rat renal impairment by downregulation of TGF-β1 and IL-1 via modulation of oxidative stress correlates with decreased apoptotic events. *Pharma Biol*. 2016;54(9):1616–1627. doi:10.3109/13880209.2015.1110599
19. Shpigelman A, Yanai S, Gal I, Yoav DL. β-Lactoglobulin–naringenin complexes: nano-vehicles for the delivery of a hydrophobic nutraceutical. *Food Hydrocoll*. 2014;40:214–224. doi:10.1016/j.foodhyd.2014.02.023
20. Villiers A. Sur la fermentation de la fécule par l'action du ferment butyrique [On the fermentation of starch by the action of butyric ferment]. *Compt Rend Fr Acad Sci*. 1891;112:435–438.
21. Matencio A, Caldera F, Cecone C, López-Nicolás JM, Trotta F. Cyclic oligosaccharides as active drugs, an updated review. *Pharmaceuticals (Basel)*. 2020;13(10):281. doi:10.3390/ph13100281
22. Stasiłowicz-Krzemien A, Gołębiewski M, Płazińska A, et al. The systems of naringenin with solubilizers expand its capability to prevent neurodegenerative diseases. *Int J Mol Sci*. 2022;23(2):755. doi:10.3390/ijms23020755
23. Xu X, Yu H, Hang L, Shao Y, Ding S, Yang X. Preparation of Naringenin/ β -cyclodextrin complex and its more potent alleviative effect on choroidal neovascularization in rats. *BioMed Res Int*. 2014;2014(23509):1–9. doi:10.1155/2014/623509
24. Shah SS, Denham LV, Elison JR, et al. Drug delivery to the posterior segment of the eye for pharmacologic therapy. *Expert Rev Ophthalmol*. 2010;5(1):75–93. doi:10.1586/eop.09.70
25. Kovalenya TA, Ilyich TV, Lapshina EA, Stępniak A, Palecz B, Zavodnik IB. Complexations of β-cyclodextrins with naringenin, naringin and catechin: thermodynamic parameters and regulation of mitochondrial functions *in vitro*. *Phys Chem Liq*. 2022;61(1):59–74. doi:10.1080/00319104.2022.2103814
26. Yan H, Zhang J, Ren S, et al. Experimental and computational studies of naringin/cyclodextrin inclusion complexation. *J Incl Phenom Macrocyclic Chem*. 2017;88(1–2):15–26. doi:10.1007/s10847-017-0704-x
27. Del Amo EM, Urtti A. Current and future ophthalmic drug delivery systems: a shift to the posterior segment. *Drug Discov Today*. 2008;13(3–4):135–143. doi:10.1016/j.drudis.2007.11.002
28. Ahmad I, Pandit J, Sultana Y, Mishra AK, Hazari PP, Aqil M. Optimization by design of etoposide loaded solid lipid nanoparticles for ocular delivery: characterization, pharmacokinetic and deposition study. *Mater Sci Eng C*. 2019;100:959–970. doi:10.1016/j.msec.2019.03.060
29. Silva M, Peng T, Zhao X, Li S, Farhan M, Zheng W. Recent trends in drug-delivery systems for the treatment of diabetic retinopathy and associated fibrosis. *Adv Drug Deliv Rev*. 2021;173:439–460. doi:10.1016/j.addr.2021.04.007
30. Kaur IP, Kakkar S. Nanotherapy for posterior eye diseases. *J Control Release*. 2014;193:100–112. doi:10.1016/j.jconrel.2014.05.031
31. Li H, Palamoor M, Jablonski MM. Poly(ortho ester) nanoparticles targeted for chronic intraocular diseases: ocular safety and localization after intravitreal injection. *Nanotoxicology*. 2016;10(8):1152–1159. doi:10.1080/17435390.2016.1181808
32. Liu Y, Wu N. Progress of nanotechnology in diabetic retinopathy treatment. *Int J Nanomed*. 2021;16:1391–1403. doi:10.2147/IJN.S294807
33. Sadasivam R, Packirisamy G, Shakya S, Goswami M. Non-invasive multimodal imaging of Diabetic Retinopathy: a survey on treatment methods and Nanotheranostics. *Nanotheranostics*. 2021;5(2):166–181. doi:10.7150/ntno.56015
34. Montoya-álvare M, Gonzalez-Perez J, Londoño ME. Diabetic retinopathy treatments based on nanotechnology. *ScienceOpen Preprints*. 2022.
35. Han H, Li S, Xu M, et al. Polymer- and lipid-based nanocarriers for ocular drug delivery: current status and future perspectives. *Adv Drug Deliv Rev*. 2023;196:114770. doi:10.1016/j.addr.2023.114770
36. Huang X, Chau Y. Intravitreal nanoparticles for retinal delivery. *Drug Discov Today*. 2019;24(8):1510–1523. doi:10.1016/j.drudis.2019.05.005
37. Tsai CH, Wang PY, Lin IC, Huang H, Liu GS, Tseng CL. Ocular drug delivery: role of degradable polymeric nanocarriers for ophthalmic application. *Int J Mol Sci*. 2018;19(9):2830. doi:10.3390/ijms19092830
38. Buosi FS, Alaimo A, Di Santo MC, et al. Resveratrol encapsulation in high molecular weight chitosan-based nanogels for applications in ocular treatments: impact on human ARPE-19 culture cells. *Int J Biol Macromol*. 2020;165(Pt A):804–821. doi:10.1016/j.ijbiomac.2020.09.234
39. Zhang X, Sun J, Yao J, et al. Effect of nanoencapsulation using poly (lactide-*co*-glycolide) (PLGA) on anti-angiogenic activity of bevacizumab for ocular angiogenesis therapy. *Biomed Pharmacother*. 2018;107:1056–1063. doi:10.1016/j.biopha.2018.08.092
40. Suen WL, Chau Y. Specific uptake of folate-decorated triamcinolone-encapsulating nanoparticles by retinal pigment epithelium cells enhances and prolongs antiangiogenic activity. *J Control Release*. 2013;167(1):21–28. doi:10.1016/j.jconrel.2013.01.004
41. Toragall V, Baskaran V. Chitosan-sodium alginate-fatty acid nanocarrier system: lutein bioavailability, absorption pharmacokinetics in diabetic rat and protection of retinal cells against H_2O_2 induced oxidative stress *in vitro*. *Carbohydr Polym*. 2021;254:117409. doi:10.1016/j.carbpol.2020.117409
42. Mahaling B, Low SWY, Ch S, et al. Next-generation nanomedicine approaches for the management of retinal diseases. *Pharmaceutics*. 2023;15(7):2005. doi:10.3390/pharmaceutics15072005
43. Manimaran V, Nivetha RP, Tamilanban T, et al. Nanogels as novel drug nanocarriers for CNS drug delivery. *Front Mol Biosci*. 2023;10:1232109. doi:10.3389/fmolb.2023.1232109
44. Jain KK. Nanobiotechnology-based drug delivery to the central nervous system. *Neurodegener Dis*. 2007;4(4):287–291. doi:10.1159/000101884
45. Kumar A, Vimal A, Kumar A. Why Chitosan? From properties to perspective of mucosal drug delivery. *Int J Biol Macromol*. 2016;91:615–622. doi:10.1016/j.ijbiomac.2016.05.054
46. Zamboulis A, Nanaki S, Michailidou G, et al. Chitosan and its derivatives for ocular delivery formulations: recent advances and developments. *Polymers*. 2020;12(7):1519.
47. Muxika A, Etxabide A, Uranga J, Guerrero P, de la Caba K. Chitosan as a bioactive polymer: processing, properties and applications. *Int J Biol Macromol*. 2017;105(Pt 2):1358–1368. doi:10.1016/j.ijbiomac.2017.07.087
48. Ways MTM, Lau WM, Khutoryanskiy VV. Chitosan and its derivatives for application in mucoadhesive drug delivery systems. *Polymers*. 2018;10(3):267. doi:10.3390/polym10030267
49. Burhan AM, Klahan B, Cummins W, et al. Posterior segment ophthalmic drug delivery: role of muco-adhesion with a special focus on chitosan. *Pharmaceutics*. 2021;13(10):1685. doi:10.3390/pharmaceutics13101685
50. Sun T, Zhou D, Mao F, Zhu Y. Preparation of low-molecular-weight carboxymethyl chitosan and their superoxide anion scavenging activity. *Eur Polym J*. 2007;43(2):652–656. doi:10.1016/j.eurpolymj.2006.11.014

51. El-Hack ME A, El-Saadony MT, Shafi ME, et al. Antimicrobial and antioxidant properties of chitosan and its derivatives and their applications: a review. *Int J Biol Macromol*. 2020;164:2726–2744. doi:10.1016/j.ijbiomac.2020.08.153
52. Zhu W, Ji Y, Wang Y, et al. Structural characterization and in vitro antioxidant activities of chondroitin sulfate purified from Andrias davidianus cartilage. *Carbohydr Polym*. 2018;196:398–404. doi:10.1016/j.carbpol.2018.05.047
53. Yang J, Shen M, Wen H, et al. Recent advance in delivery system and tissue engineering applications of chondroitin sulfate. *Carbohydr Polym*. 2020;230:115650. doi:10.1016/j.carbpol.2019.115650
54. Amhare AF, Lei J, Deng H, Lv Y, Han J, Zhang L. Biomedical application of chondroitin sulfate with nanoparticles in drug delivery systems: systematic review. *J Drug Target*. 2021;29(3):259–268. doi:10.1080/1061186X.2020.1833018
55. Belalcázar-Rey S, Sánchez Huerta V, Ochoa-Tabares JC, et al. Efficacy and safety of sodium hyaluronate/chondroitin sulfate preservative-free ophthalmic solution in the treatment of dry eye: a clinical trial. *Curr Eye Res*. 2021;46(7):919–929. doi:10.1080/02713683.2020.1849733
56. Jiang S, Franco YL, Zhou Y, Chen J. Nanotechnology in retinal drug delivery. *Int J Ophthalmol*. 2018;11(6):1038–1044. doi:10.18240/ijo.2018.06.23
57. Jardim KV, Siqueira JLN, Báo SN, Sousa MH, Parize AL. The role of the lecithin addition in the properties and cytotoxic activity of chitosan and chondroitin sulfate nanoparticles containing curcumin. *Carbohydr Polym*. 2020;227:115351. doi:10.1016/j.carbpol.2019.115351
58. Rezazadeh M, Parandeh M, Akbari V, Ebrahimi Z, Taheri A. Incorporation of rosuvastatin-loaded chitosan/chondroitin sulfate nanoparticles into a thermosensitive hydrogel for bone tissue engineering: preparation, characterization, and cellular behavior. *Pharm Dev Technol*. 2018;24(3):357–367. doi:10.1080/10837450.2018.1484765
59. Yeh M, Cheng K, Hu C, Huang Y, Young J. Novel protein-loaded chondroitin sulfate–chitosan nanoparticles: preparation and characterization. *Acta Biomater*. 2011;7(10):3804–3812. doi:10.1016/j.actbio.2011.06.026
60. Valentino C, Vigani B, Fedeli I, et al. Development of alginate-spermidine micro/nanogels as potential antioxidant and anti-inflammatory tool in peripheral nerve injuries. Formulation studies and physico-chemical characterization. *Int J Pharm*. 2022;626:122168.
61. Vigani B, Valentino C, Sandri G, Caramella CM, Ferrari F, Rossi S. Spermidine crosslinked gellan gum-based "hydrogel nanofibers" as potential tool for the treatment of nervous tissue injuries: a formulation study. *Int J Nanomed*. 2022;17:3421–3439. doi:10.2147/IJN.S368960
62. Valentino C, Vigani B, Zucca G, et al. Formulation development of collagen/chitosan-based porous scaffolds for skin wounds repair and regeneration. *Int J Biol Macromol*. 2023;242(Part 3):125000. doi:10.1016/j.ijbiomac.2023.125000
63. Yu Z, Yu D, Dong J, Xia W. Ultrasound-reinforced encapsulation of proanthocyanidin by chitosan-chondroitin sulfate nanosystem. *Food Hydrocoll*. 2022;132:107872. doi:10.1016/j.foodhyd.2022.107872
64. Kowluru RA, Tang J, Kern TS. Abnormalities of retinal metabolism in diabetes and experimental galactosemia. VII. Effect of long-term administration of antioxidants on the development of retinopathy. *Diabetes*. 2001;50(8):1938–1942. doi:10.2337/diabetes.50.8.1938
65. Fahmideh F, Marchesi N, Campagnoli LIM, et al. Effect of troxerutin in counteracting hyperglycemia-induced VEGF upregulation in endothelial cells: a new option to target early stages of diabetic retinopathy? *Front Pharmacol*. 2022;13:951833. doi:10.3389/fphar.2022.951833
66. Liao Y, Fang Y, Sun J, Dou G. Senescent endothelial cells: a potential target for diabetic retinopathy. *Angiogenesis*. 2024;27(4):663–679. doi:10.1007/s10456-024-09943-7
67. Wen J, Liu B, Yuan E, Ma Y, Zhu Y. Preparation and physicochemical properties of the complex of naringenin with hydroxypropyl-beta-cyclodextrin. *Molecules*. 2010;15(6):4401–4407. doi:10.3390/molecules15064401
68. Xu XR, Yu HT, Hang L, Shao Y, Ding SH, Yang XW. Preparation of naringenin/ β-cyclodextrin complex and its more potent alleviative effect on choroidal neovascularization in rats. *Biomed Res Int*. 2014;2014:623509.
69. Yang L, Ma S, Zhou S, et al. Preparation and characterization of inclusion complexes of naringenin with β-cyclodextrin or its derivative. *Carbohydr Polym*. 2013;98(1):861–869. doi:10.1016/j.carbpol.2013.07.010
70. Allmendinger A, Butt YL, Mueller C. Intraocular pressure and injection forces during intravitreal injection into enucleated porcine eyes. *Eur J Pharm Biopharm*. 2021;166:87–93. doi:10.1016/j.ejpb.2021.06.001
71. Sapino S, Peira E, Chirio D, et al. Thermosensitive nanocomposite hydrogels for intravitreal delivery of cefuroxime. *Nanomaterials (Basel)*. 2019;9(10):1461. doi:10.3390/nano9101461
72. Ruggeri M, Sánchez-Espejo R, Casula L, et al. Clay-based hydrogels as drug delivery vehicles of curcumin nanocrystals for topical application. *Pharmaceutics*. 2022;14(12):2836. doi:10.3390/pharmaceutics14122836
73. Debele TA, Mekuria SL, Tsai HC. Polysaccharide based nanogels in the drug delivery system: application as the carrier of pharmaceutical agents. *Mater Sci Eng C Mater Biol Appl*. 2016;68:964–981. doi:10.1016/j.msec.2016.05.121
74. Wu D, Zhu L, Li Y, et al. Chitosan-based Colloidal Polyelectrolyte Complexes for Drug Delivery: a Review. *Carbohydr Polym*. 2020;238:116126. doi:10.1016/j.carbpol.2020.116126
75. Bonaccorso A, Carbone C, Tomasello B, et al. Optimization of dextran sulfate/poly-l-lysine based nanogels polyelectrolyte complex for intranasal ovalbumin delivery. *J Drug Deliv Sci Technol*. 2021;65:102678. doi:10.1016/j.jddst.2021.102678
76. Luo Y, Wang Q. Recent development of chitosan-based polyelectrolyte complexes with natural polysaccharides for drug delivery. *Int J Biol Macromol*. 2014;64:353–367. doi:10.1016/j.ijbiomac.2013.12.017
77. Quiñones JP, Peniche H, Peniche C. Chitosan based self-assembled nanoparticles in drug delivery. *Polymers*. 2018;10(3):235. doi:10.3390/polym10030235
78. Jardim KV, Joanitti GA, Azevedo RB, Parize AL. Physico-chemical characterization and cytotoxicity evaluation of curcumin loaded in chitosan/chondroitin sulfate nanoparticles. *Mater Sci Eng C Mater Biol Appl*. 2015;56:294–304. doi:10.1016/j.msec.2015.06.036
79. Schatz C, Lucas J, Viton C, Domard A, Pichot C, Delair T. Formation and properties of positively charged colloids based on polyelectrolyte complexes of biopolymers. *Langmuir*. 2004;20(18):7766–7778. doi:10.1021/la049460m
80. Schatz C, Domard A, Viton C, Pichot C, Delair T. Versatile and efficient formation of colloids of biopolymer-based polyelectrolyte complexes. *Biomacromolecules*. 2004;5(5):1882–1892.
81. Wu D, Ensinas A, Verrier B, et al. Carbohydr. *Polym*. 2017;172:265–274.
82. Wu D, Delair T. Stabilization of chitosan/hyaluronan colloidal polyelectrolyte complexes in physiological conditions. *Carbohydr Polym*. 2015;119:149–158. doi:10.1016/j.carbpol.2014.11.042
83. Jonassen H, Kjøniksen AL, Hiorth M. Effects of ionic strength on the size and compactness of chitosan nanoparticles. *Colloid Polym Sci*. 2012;290(10):919–929. doi:10.1007/s00396-012-2604-3

84. Hu B, Pan C, Sun Y, et al. Optimization of fabrication parameters to produce chitosan−tripolyphosphate nanoparticles for delivery of tea catechins. *J Agric Food Chem*. 2008;56(16):7451–7458. doi:10.1021/jf801111c
85. Gan Q, Wang T, Cochrane C, McCarron P. Modulation of surface charge, particle size and morphological properties of chitosan–TPP nanoparticles intended for gene delivery. *Colloids Surf B*. 2005;44(2–3):65–73. doi:10.1016/j.colsurfb.2005.06.001
86. Bugnicourt L, Alcouffe P, Ladavière C. Elaboration of chitosan nanoparticles: favorable impact of a mild thermal treatment to obtain finely divided, spherical, and colloidally stable objects. *COLSUA*. 2014;457:476–486.
87. Huang Y, Lapitsky Y. On the kinetics of chitosan/tripolyphosphate micro- and nanogel aggregation and their effects on particle polydispersity. *J Colloid Interface Sci*. 2017;486:27–37. doi:10.1016/j.jcis.2016.09.050
88. Slyusareva E, Gerasimova M, Plotnikov CA, Sizykh A. Spectral study of fluorone dyes adsorption on chitosan-based polyelectrolyte complexes. *J Colloid Interface Sci*. 2014;417:80–87. doi:10.1016/j.jcis.2013.11.016
89. Liang T, Zhang Z, Jing P. Black rice anthocyanins embedded in self-assembled chitosan/chondroitin sulfate nanoparticles enhance apoptosis in HCT-116 cells. *Food Chem*. 2019;301:125280. doi:10.1016/j.foodchem.2019.125280
90. Donahue ND, Acar H, Wilhelm S. Concepts of nanoparticle cellular uptake, intracellular trafficking, and kinetics in nanomedicine. *Adv Drug Deliv Rev*. 2019;143:68–96. doi:10.1016/j.addr.2019.04.008
91. Ta Q, Ting J, Harwood S, et al. Chitosan nanoparticles for enhancing drugs and cosmetic components penetration through the skin. *Eur J Pharm Sci*. 2021;160:105765. doi:10.1016/j.ejps.2021.105765
92. Sakurai E, Ozeki H, Kunou N, Ogura Y. Effect of particle size of polymeric nanospheres on intravitreal kinetics. *Ophthalmic Res*. 2001;33 (1):31–36. doi:10.1159/000055638
93. Kiilll CP, Barud HDS, Santagneli SH. Synthesis and factorial design applied to a novel chitosan/sodium polyphosphate nanoparticles via ionotropic gelation as an RGD delivery system. *Carbohydr Polym*. 2017;157:1695–1702. doi:10.1016/j.carbpol.2016.11.053
94. Amadio M, Pascale A, Cupri S, et al. Nanosystems based on siRNA silencing HuR expression counteract diabetic retinopathy in rat. *Pharmacol Res*. 2016;111:713–720. doi:10.1016/j.phrs.2016.07.042
95. Kiio TM, Park S. Physical properties of nanoparticles do matter. *J Pharm Investig*. 2021;51(1):35–51. doi:10.1007/s40005-020-00504-w
96. Pereira AD, Silva PM, Oliveira JL, Oliveira HC, Fraceto LF. Chitosan nanoparticles as carrier systems for the plant growth hormone gibberellic acid. *Colloids Surf B*. 2017;150:141–152. doi:10.1016/j.colsurfb.2016.11.027
97. Ribeiro EF, de Barros-Alexandrino TT, Assis OBG. Chitosan and crosslinked chitosan nanoparticles: synthesis, characterization and their role as Pickering emulsifiers. *Carbohydr Polym*. 2020;250:116878. doi:10.1016/j.carbpol.2020.116878
98. Falke S, Betzel C. Dynamic Light Scattering (DLS). In: Tavares A, Limão-Vieira P, Pereira P, editors. *Radiation in Bioanalysis*. Vol. 8. Springer. Cham. 2019;173–193.
99. Sun H, Jiao R, An G, Xu H, Wang D. Influence of particle size on the aggregation behavior of nanoparticles: role of structural hydration layer. *Environ Sci*. 2021;103:33–42. doi:10.1016/j.jes.2020.10.007
100. Feyzioglu G, Tornuk F. Development of chitosan nanoparticles loaded with summer savory (Satureja hortensis L.) essential oil for antimicrobial and antioxidant delivery applications. *LWT*. 2016;70:104–110. doi:10.1016/j.lwt.2016.02.037
101. McComiskey KPM, Tajber L. Comparison of particle size methodology and assessment of nanoparticle tracking analysis (NTA) as a tool for live monitoring of crystallisation pathways. *Eur J Pharm Biopharm*. 2018;130:314–326. doi:10.1016/j.ejpb.2018.07.012
102. Waiprib Y, Ingrungruengluet P, Worawattanamateekul W. Nanoparticles based on chondroitin sulfate from tuna heads and chitooligosaccharides for enhanced water solubility and sustained release of curcumin. *Polymers*. 2023;15(4):834. doi:10.3390/polym15040834
103. Singh BN, Veeresh V, Mallick SP, Sinha S, Rastogi A, Srivastava P. Generation of scaffold incorporated with nanobioglass encapsulated in chitosan/chondroitin sulfate complex for bone tissue engineering. *Int J Biol Macromol*. 2020;153:1–16. doi:10.1016/j.ijbiomac.2020.02.173
104. Chen LJ, Ito S, Kai H, et al. Microfluidic co-cultures of retinal pigment epithelial cells and vascular endothelial cells to investigate choroidal angiogenesis. *Sci Rep*. 2017;7(1):3538. doi:10.1038/s41598-017-03788-5
105. Esmaeili A, Asgari A. In vitro release and biological activities of *Carum copticum* essential oil (CEO) loaded chitosan nanoparticles. *Int J Biol Macromol*. 2015;81:283–290. doi:10.1016/j.ijbiomac.2015.08.010
106. Mrugacz M, Bryl A, Zorena K. Retinal vascular endothelial cell dysfunction and neuroretinal degeneration in diabetic patients. *J Clin Med*. 2021;10(3):458. doi:10.3390/jcm10030458
107. Wareham LK, Calkins DJ. The neurovascular unit in glaucomatous neurodegeneration. *Front Cell Dev Biol*. 2020;8:452. doi:10.3389/fcell.2020.00452
108. Eyre JJ, Williams RL, Levis HJ. A human retinal microvascular endothelial-pericyte co-culture model to study diabetic retinopathy in vitro. *Exp Eye Res*. 2020;201:108293. doi:10.1016/j.exer.2020.108293
109. Astolfi G, Ciavarella C, Valente S, et al. Human glial müller and umbilical vein endothelial cell coculture as an in vitro model to investigate retinal oxidative damage. A morphological and molecular assessment. *Microsc Res Tech*. 2023;86(4):439–451. doi:10.1002/jemt.24284
110. Jiang L, Yang J, Wang Q, Ren L, Zhou J. Physicochemical properties of catechin/β-cyclodextrin inclusion complex obtained via co-precipitation. *CYTA J Food*. 2019;17(1):544–551. doi:10.1080/19476337.2019.1612948
111. Owen SC, Doak AK, Ganesh AN, et al. Colloidal drug formulations can explain "bell-shaped" concentration-response curves. *ACS Chem Biol*. 2014;9(3):777–784. doi:10.1021/cb4007584
112. Govoni S, Battaini F, Lucchi L, Pascale A, Trabucchi M. PKC translocation in rat brain cortex is promoted in vivo and in vitro by α-Glycerylphosphorylcholine, a cognition-enhancing drug a. *Ann N Y Acad Sci*. 1993;695(1):307–310. doi:10.1111/j.1749-6632.1993.tb23072.x
113. Pascale A, Milano S, Corsico N, et al. Protein kinase C activation and anti-amnesic effect of acetyl-L-carnitine: in vitro and in vivo studies. *Eur J Pharmacol*. 1994;265(1–2):1–7. doi:10.1016/0014-2999(94)90216-X
114. Semalty A, Tanwar YS, Semalty M. Preparation and characterization of cyclodextrin inclusion complex of naringenin and critical comparison with phospholipid complexation for improving solubility and dissolution. *J Therm Anal Calorim*. 2014;115(3):2471–2478. doi:10.1007/s10973-013-3463-y
115. Jin X, Zhang Z, Sun E, Li S, Jia X. Statistically designed enzymatic hydrolysis of an icariin/β-cyclodextrin inclusion complex optimized for production of icaritin. *Acta Pharm Sin B*. 2012;2(1):83–89. doi:10.1016/j.apsb.2011.12.004
116. Wang X, Luo Z, Xiao Z. Preparation, characterization, and thermal stability of β-cyclodextrin/soybean lecithin inclusion complex. *Carbohydr Polym*. 2014;101:1027–1032. doi:10.1016/j.carbpol.2013.10.042

117. Jambhekar SS, Breen P. Cyclodextrins in pharmaceutical formulations I: structure and physicochemical properties, formation of complexes, and types of complex. *Drug Discov Today*. 2016;21(2):356–362. doi:10.1016/j.drudis.2015.11.017
118. Sadaquat H, Akhtar M. Comparative effects of β-cyclodextrin, HP-β-cyclodextrin and SBE_7-β-cyclodextrin on the solubility and dissolution of docetaxel via inclusion complexation. *J Incl Phenom Macrocyclic Chem*. 2020;96(3–4):333–351. doi:10.1007/s10847-020-00977-0
119. Dehghani A, Bahlakeh G, Ramezanzadeh B. Synthesis of a non-hazardous/smart anti-corrosion nano-carrier based on beta-cyclodextrin-zinc acetylacetonate inclusion complex decorated graphene oxide (β-CD-ZnA-MGO). *J Hazard Mater*. 2020;398:122962. doi:10.1016/j.jhazmat.2020.122962
120. Mashaqbeh H, Obaidat R, Al-Shar'I N. Evaluation and characterization of curcumin-β-cyclodextrin and cyclodextrin-based nanosponge inclusion complexation. *Polymers*. 2021;13(23):4073. doi:10.3390/polym13234073
121. Alizadeh N, Nazari F. Thymol essential oil/ β-cyclodextrin inclusion complex into chitosan nanoparticles: improvement of thymol properties in vitro studies. *J Mol Liq*. 2022;346:118250. doi:10.1016/j.molliq.2021.118250
122. Bensouiki S, Belaib F, Sindt M, et al. Synthesis of cyclodextrins-metronidazole inclusion complexes and incorporation of metronidazole - 2-hydroxypropyl-β-cyclodextrin inclusion complex in chitosan nanoparticles. *J Mol Struct*. 2022;1247:131298. doi:10.1016/j.molstruc.2021.131298
123. Karpour M, Alizadeh N. Physicochemical characterization and in vitro evaluation of mesalazine/β-cyclodextrin inclusion complex loaded into chitosan nanoparticles. *Polym Bull*. 2022;80(2):1–19.
124. Hancock BC, Parks M. What is the True Solubility Advantage for Amorphous Pharmaceuticals? *Pharm Res*. 2000;17(4):397–404. doi:10.1023/A:1007516718048
125. Zhu Z, Luo Y, Liu Y, et al. Inclusion of chrysin in β-cyclodextrin and its biological activities. *J Drug Deliv Sci Technol*. 2016;31:176–186. doi:10.1016/j.jddst.2016.01.002
126. Liang Y, Hou D, Ni Z, Cao M, Cai L. Preparation, characterization of naringenin, β-cyclodextrin and carbon quantum dot antioxidant nanocomposites. *Food Chem*. 2016;375:131646. doi:10.1016/j.foodchem.2021.131646
127. Donati S, Caprani SM, Airaghi G, et al. Vitreous substitutes: the present and the future. *BioMed Res Int*. 2014;2014:351804. doi:10.1155/2014/351804
128. Canioni R, Reynaud F, Leite-Nascimento T, et al. Tiny dexamethasone palmitate nanoparticles for intravitreal injection: optimization and in vivo evaluation. *Int J Pharm*. 2021;600:120509. doi:10.1016/j.ijpharm.2021.120509
129. Wu MY, Yiang GT, Lai TT, Li CJ. The Oxidative Stress and Mitochondrial Dysfunction during the Pathogenesis of Diabetic Retinopathy. *Oxid Med Cell Longev*. 2018;2018(1):3420187. doi:10.1155/2018/3420187
130. Rossino MG, Casini G. Nutraceuticals for the Treatment of Diabetic Retinopathy. *Nutrients*. 2019;11(4):771. doi:10.3390/nu11040771
131. Matos AL, Bruno DF, Ambrósio AF, Santos PF. The benefits of flavonoids in diabetic retinopathy. *Nutrients*. 2020;12(10):3169. doi:10.3390/nu12103169
132. Chiang Y, Chen H, Chang Y, et al. Protective effects of fucoxanthin on high glucose- and 4-Hydroxynonenal (4-HNE)-induced injury in human retinal pigment epithelial cells. *Antioxidants*. 2020;9(12):1176. doi:10.3390/antiox9121176
133. Huang X, Huang X, Gong Y, Xiao H, McClements DJ, Hu K. Enhancement of curcumin water dispersibility and antioxidant activity using core-shell protein-polysaccharide nanoparticles. *Food Res Int*. 2016;87:1–9. doi:10.1016/j.foodres.2016.06.009
134. Huang M, Khor E, Lim LY. Uptake and cytotoxicity of chitosan molecules and nanoparticles: effects of molecular weight and degree of deacetylation. *Pharm Res*. 2004;21(2):344–353. doi:10.1023/B:PHAM.0000016249.52831.a5
135. Liu Y, Ying D, Cai Y, Le X. Improved antioxidant activity and physicochemical properties of curcumin by adding ovalbumin and its structural characterization. *Food Hydrocoll*. 2017;72:304–311. doi:10.1016/j.foodhyd.2017.06.007
136. Zaki SS, Ibrahim MN, Katas H. Particle size affects concentration-dependent cytotoxicity of chitosan nanoparticles towards mouse hemato-poietic stem cells. *J Nanotechnol*. 2015;2015:etal919658.